Spring 2013

Gas and water flow through nanoscale porous media

Songyuan Liu

Department:

GAS AND WATER FLOW THROUGH

NANOSCALE POROUS MEDIA

by

SONGYUAN LIU

A THESIS

Presented to the Faculty of the Graduate School of the

MISSOURI UNIVERSITY OF SCIENCE AND TECHNOLOGY

In Partial Fulfillment of the Requirements for the Degree

Master of Science

in

PETROLEUM ENGINEERING

2013

Approved by

Baijun Bai, Advisor
Ralph E. Flori
Runar Nygaard

ABSTRACT

This work provides a lab experiment to describe the fluid diffusion in nanoscale porous media. By using ideal ceramic membranes which have uniform pore size in nanoscale and homogeneous pore distribution instead of shale or tight sandstone which have various pore sizes and complicated pore distribution and structure, a better understanding of fluid flow through nanoscale porous media could be gained..

Core flooding test were conducted by injecting nitrogen and water separately to describe gas and liquid flow in nanoscale porous media. With all the other factors known or controlled, pressure and flow rate were measured to calculate permeability. By the difference of the ability that gas and fluid pass through the different sizes of porous media, we can better understand how the nanoscale pore size in unconventional reservoirs affects the petroleum production.

Lab data were fitted into two derived models for fluid diffusion in nano-scale porous media by Javadpour and Florence. Lab data made a good fit with Javadpour's model except a slight difference of slope with a reasonable tangential momentum accommodation coefficient. However, permeability results getting from Florence's model were in different magnitude from lab data which might owing to high Knudsen number due to the extra small pore size in this lab.

ACKNOWLEDGEMENTS

I would like to express my gratitude to my advisor Dr. Baojun Bai for his guidance throughout the completion of this work and also for his criticism and encouragement on my academic and life which make me to be a better researcher as well as a better person. In addition, I would like to thank my committee members Dr. Ralph Flori and Dr. Runar Nygaard for their helpful advice and patient instruction.

I also appreciate the help from my friends. Hao Zhang and Yongpeng Sun help me with all my lab model setup and give me all kinds of advice. SEM figures will not be done without the help from Qianyao Li. Chaohua Guo share the literature and ideas with me. Thank you all for being there when I need help. At last I wish to express my love and gratitude to my beloved families; for their understanding and support, through the duration of my studies.

Lastly, I wish to convey my thanks to RPSEA which provided the funding for this project through the "Ultra-Deepwater and Unconventional Natural Gas and Other Petroleum Resources" program authorized by the U.S. Energy Policy Act of 2005.

TABLE OF CONTENTS

LIST OF ILLUSTRATIONS

Page

LIST OF TABLES

Page

NOMENCLATURE

4.1 Darcy's law based Klinkenberg diffusion

P_m = mean pressure, atm

P_1 = upstream pressure, atm

P_2 = downstream pressure, atm

K_a = apparent permeability, md

L = core length, cm

μ = viscosity, cp

A = area, cm2

Q = gas flow rate, cc/s

4.2 Kozeny-Carman equation

K = permeability, nm^2

Φ = prosity

d_p = pore diameter, nm

τ = tuotorsity

4.3 Florence's nano flow model

K_a = apparent gas permeability, md

K_n = Knudsen number, dimensionless

k_∞ = equivalent liquid permeability or Klinkenberg-corrected permeability, md

c = Proportionality constant

$\alpha(K_n)$ = Dimensionless term in the rarefaction coefficient

4.4 Javadpour's nano flow model

k_{app} = apparent permeability, m2

r = pore radius, m

μ = viscosity, Pa.s

M = molar mass, kg/kmol

q = flow rate, m3/s

T = temperature, K

ρ_{avg} = mean density, kg/m3

F = theoretical dimensionless coefficient

α = tangential momentum accommodation coefficient,

P_{avg} = mean pressure, kPa

1. INTRODUCTION

Unconventional resources are occupying more and more energy consumption due to the increasing energy demand over the earth and the depletion of conventional resources. The major reason that activates but also limits the production of unconventional resources is the immature technology. (BE Law et al., 2005) My work is to conduct a theoretical study measuring gas and water transport through nano scale membranes to give a better understanding of fluid diffusion in unconventional reservoirs which provides a fundamental basis for new technologies which lead to a better recovery.

Due to the extra low permeability and the complicated pore size distribution of the unconventional reservoir rock, measurements are hard to conduct and results are hard to define. (T McCallister, 2000) Simulation works were done by setting up different media and different algorithm. The porous media is defined from micro scale to nano scale or the combination of both while the algorithms are slightly different derived from fluid flow equation. (G Karniadakis et al., 2005)

From micro scale to nano scale, the reports are fewer and more inconformity. The pattern of fluid flow in nano scale is not clear for now and the transition between Klinkenburg diffusion and Knudsen diffusion is not quantified. More theoretical studies should be conducted to provide a fundamental basis considering different methods to derive fluid flow equation under tiny pore size led to the inconformity of studies of unconventional resources. According to the former work focus on nanoscale, Subrata Roy etc. once used nanoscale pore sized membrane to determine gas transport characteristics

through a carbon nanotubule. Gas transport was measured in membranes with the smallest pore size to be 200nm.

This study measured both water and gas transport using membranes with pore size from 20 to 100nm. The pore size range is appropriate to be considered as simplified model for unconventional reservoir rock, most of all shale which is showed in Figure 1.1. As what is circled by black box, different kind of shlaes have pore sizes from less than 10nm to 100nm while tight sandstone range from 10nm to 1000nm. Both liquid and gas measurements give comprehensive lab results for application in tight oil and gas. Membranes were better to be identified and described due to the uniformity of the membranes.

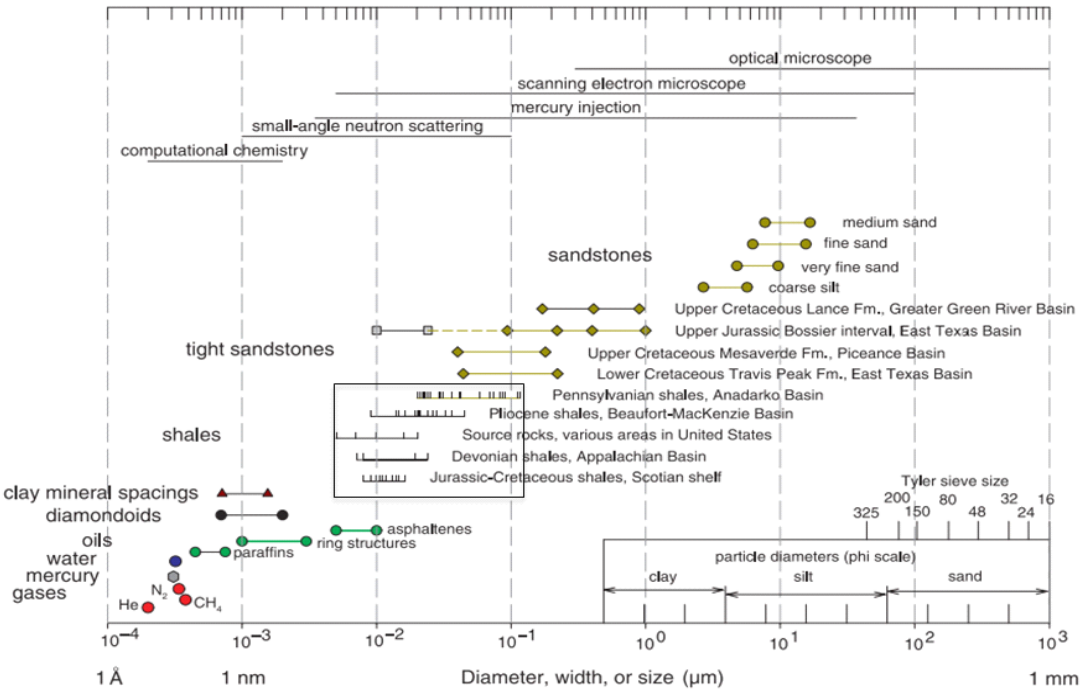

Figure 1.1 Sizes of molecules and pore throats in siliciclastic rocks on a logarithmic scale covering seven orders of magnitude (Philip H. Nelson, 2009)

Scanning election microscope (SEM) figures were taken to characterize membranes and give a precise value to either pore size or pore density. Kozeny-Carman equation was used to roughly evaluate the permeability according to the SEM data. Permeability was calculated by lab data from water measurement under Darcy's law. According to the diffusion theory that the tinier the pore size is to the transport molecule mean free path the more Knudsen diffusion occurs. Lab data from gas measurement was dealed with Klinkenberg diffusion based on Darcy's law as well as two models in which Knudsen diffusion was introduced--Javadpour's model and Florence's model.

2. LITERATURE REVIEW

To provide context and background for the thesis research, this chapter will provide 1) a brief introduction and economy outlook of unconventional gas and oil, 2) the concept of permeability and the description of reservoir, 3) current lab methods to measure permeability, 4) current fluid diffusion models when Knudsen diffusion occurs.

2.1 UNCONVENTIONAL RESOURCES

Unconventional resources are those that have been bypassed for economic reasons comparing to conventional oil and gas for decades. The improvements in geophysical and geochemical exploration, and drilling and completion technologies since the early 1990s have opened up new resources in the United States both onshore and offshore.

Unconventional resources include tight oil and gas, shale oil and gas, coalbed methane, heavy oil, deep and ultra deep water plays and gas hydrates and are widely distributed around the world as showed in Figure 2.1. Specific techniques and strategies are required to develop different kind of unconventional resources for economical and environmental reasons.

2.1.1 Coalbed Methane. Development of coalbed methane (CBM) began in the mid 1980s in the San Juan Basin, New Mexico (BS Kelso et al. 1988). The largest and most mature CBM producing regions are the San Juan Basin, Black Warrior Basin in Alabama and the Powder RiverBasin in Wyoming and Montana, but resources in the Appalachian

basins, Illinois Basin, Gulf Coast, Mid Continent (Kansas, Oklahoma and Arkansas) and other Rocky Mountain basins are also being economically produced (Figure 2.2). Production from coal seams requires a series of vertical wells that pump groundwater to the surface to reduce the hydrostatic pressure on the coal releasing the methane. During initial stages of production large volumes of produced water are pumped to the surface. As the coal seam gradually releases the methane, the volume of water produced diminishes over the life of the well, typically a period of 20 years.

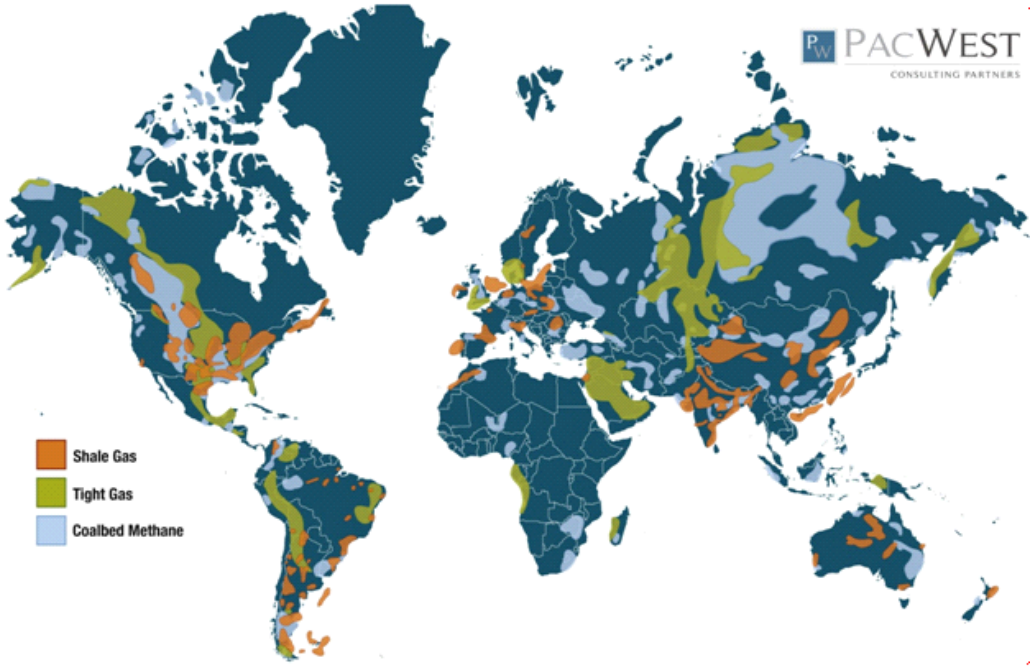

Figure 2.1 Presence of unconventional resources types around the world (PACWEST)

Controlling factors for CBM production include permeability, fractures, gas migration, coal maturation, coal distribution, geologic structure and basin tectonics (RM Flores, 1998). Natural fracturing is primarily related to geologic structure, regional

tectonics and coal maturation or coal rank. Coal is derived from plant material accumulated in bogs and swamps. Maturation occurs as the plant and woody material is compressed and hardened by heat by and overburden pressure changing from peat to lignite to bituminous and finally anthracite coal.

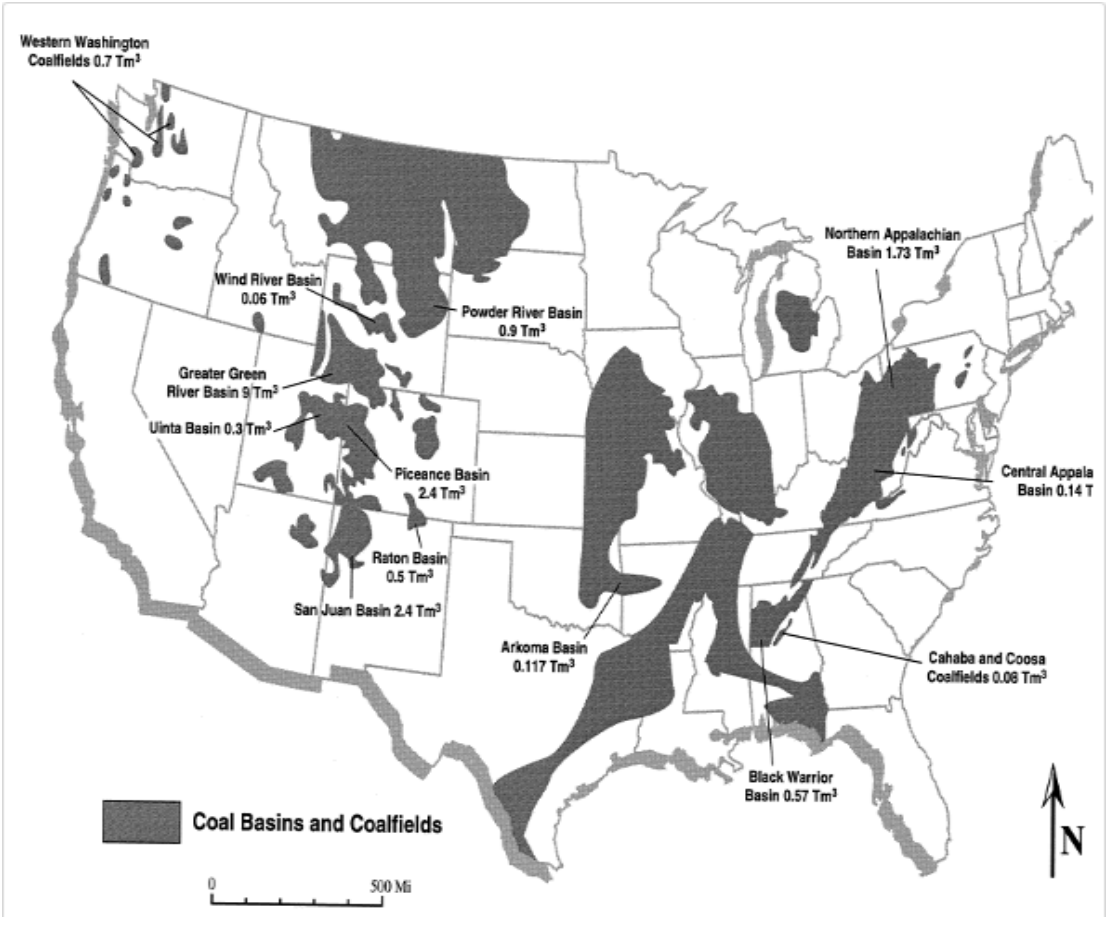

Figure 2.2 A map showing coal basins/coalfields in the United States and estimates of in-place coalbed methane resource modified from ICF Resources (1990), Tyler et al. (1997) and Bibler et al. (1998)

Two processes are primarily responsible for coalbed methane development, biogenesis and thermo genesis. Biogenic methane is produced naturally by the action of

organisms ingesting the carbon material in the decaying plant material. Thermogenic methane is produced by oxidation reactions caused by increased temperature in the maturation process. Biogenic processes tend to form at lower temperatures in the lignite to sub-bituminous coal ranks, while bituminous and anthracite coals are formed by thermo genesis. Coal has low permeability, and fluids tend to migrate through secondary permeability zones such as natural fractures or cleats.

During CBM production water flow causes the hydrostatic pressure within the coal seam to decrease, allowing gas to be desorbed from the surface of the cleat and migrate through the cleat network to the wellbore. Less methane is produced from anthracite coal, because the coal has little porosity and the water remains in the matrix. CBM production from the Rocky Mountain States is mainly from sub-bituminous and bituminous coals. Because sub-bituminous coals are softer and less competent, they are typically completed using vertical wellbores. Submersible pumps are commonly used to pump the water from the coal seams in order to desorb or release the methane. If the cleat system is not fully developed, low-pressure stimulation techniques are used to fracture the coal seam and open the cleat network.

CBM production technologies are well established, but environmental, regulatory and cultural factors related to water use and disposal often determine the economic feasibility of production wells and fields (Figure 2.3). Water management issues including availability, water rights, disposal, treatment and beneficial reuse are the main factors that CBM operators must deal with. Regulations and water rights vary from state

to state, and are often hotly contested in the Rocky Mountain States. In the past ten years numerous research projects sponsored both by the Department of Energy and industry have looked at technologies to cost-effectively treat CBM produced water to meet state and federal regulations for beneficial use. The ultimate goal is to establish a range of technologies adapted to the range of total dissolved solids (TDS) (salts and metals), and contaminants (organic and toxic) in CBM produced water that will allow the water to be used for agriculture, municipal, industrial, and oil and gas production activities.

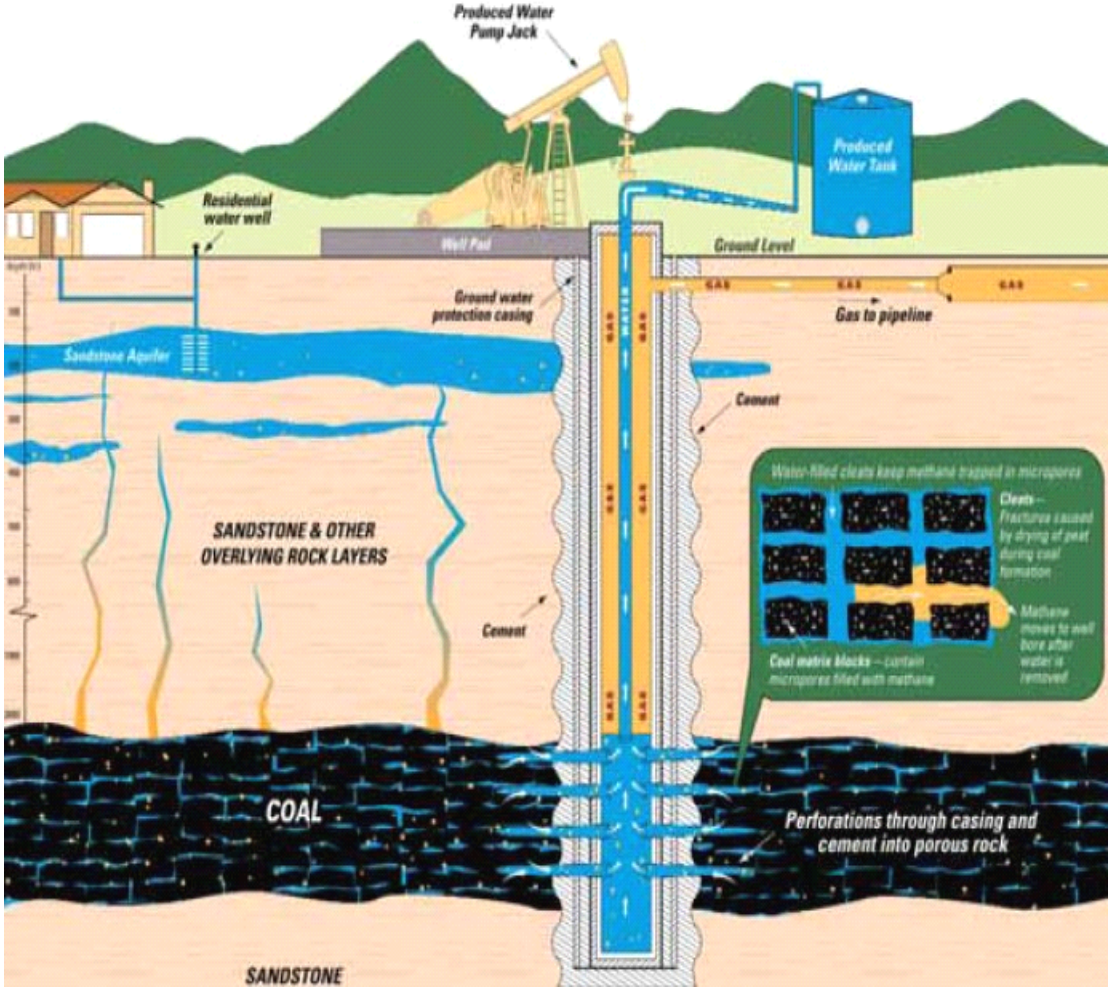

Figure 2.3 Typical Coalbed Methane Well (Ecos Consulting)

Currently the main technologies being addressed are desalination using reversed osmosis, ion exchange, nanofiltration membranes, capacitive deionization, electro dialysis, and electro dialysis reversal. Development of longer lasting, low-cost and self-cleansing membranes has been an important part of the research. Treatment and beneficial use of CBM produced water would fulfill two goals; compliance with regulatory requirements by states and federal agencies, and providing a secondary income source from the sale of the produced water.

2.1.2 Heavy Oil. Heavy oil is defined as oil with an API gravity less than 20º. API specific gravity is a measure of the viscosity or the internal resistance of a fluid to flow. Heavy oil forms from crude oil by processes of degradation through exposure to bacteria, water, or air resulting in a loss of the lighter oil fractions, leaving behind the heavy fractions. Below 10º API heavy oil does not flow and is referred to as asphalt or tar sand. Bitumen is the mixture of organic petroleum liquids that are viscous, black and sticky, and must be heated before it will flow. Worldwide resources of heavy oil are greater than conventional oil resources (Figure 2.4).

The largest heavy oil reservoirs are in Venezuela, China and Canada. However, extensive heavy oil deposits are found in California and East Texas. Oil recovery from heavy oil and bitumen reservoirs is much more difficult than that from conventional oil reservoirs. This is mainly because heavy oil or bitumen is partially or completely immobile under reservoir conditions due to its extremely high viscosity, which creates

special production challenges. Common components of heavy oil are asphaltene and paraffin molecules, which must be kept in solution to produce the heavy oil. Thermal recovery methods, including steam injection, cyclic steam and in-situ combustion are the most common technologies that have been used in California for several decades. Improved thermal recovery methods developed primarily in Canada include, steam assisted gravity drainage (SAGD), vapor extraction, and toe-to heel air injection (THAI). Thermal recovery technologies are generally considered as tertiary recovery.

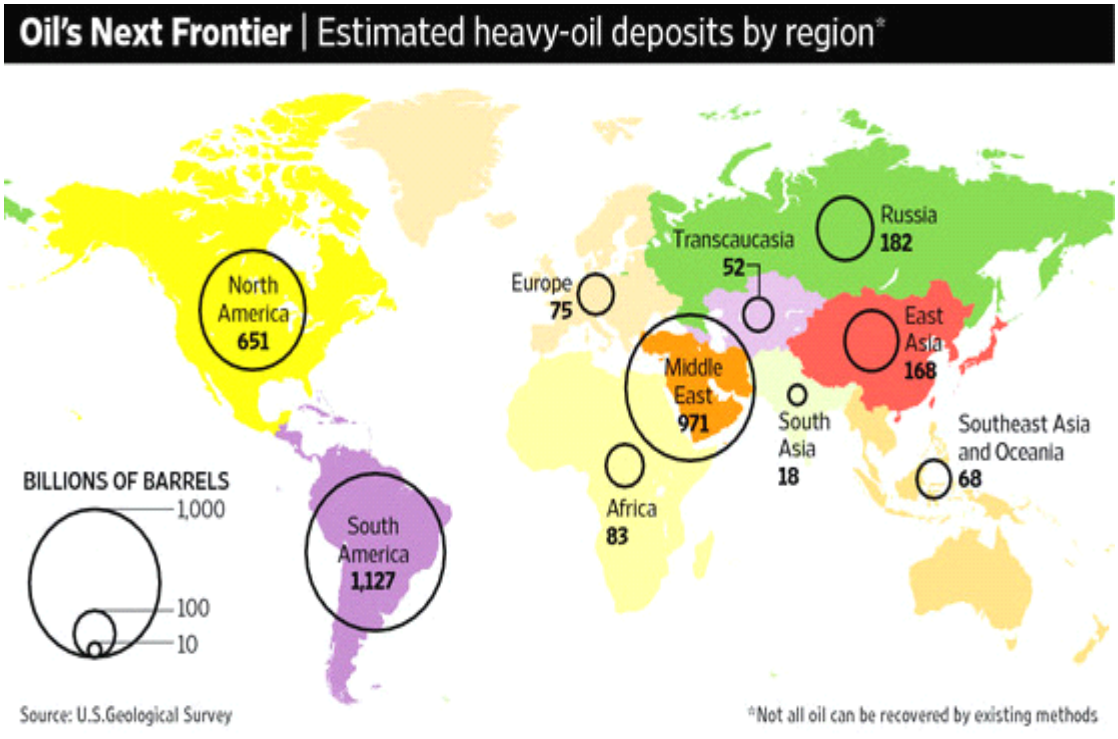

Figure 2.4 Worldwide estimated heavy-oil deposits by region (U.S Geological Survey)

More recently cold heavy oil production with sand (CHOPS) has been developed for extracting heavy oil and tar sands in Canada. In this process sand is used to enhance the

productivity of the well. Application of CHOPS in unconsolidated sandstones has led to its use in shallow heavy oil reservoirs on the Alaska North Slope. Because of the unique properties of these Alaskan reservoirs and the frozen climate, CHOPS is essentially used as the primary recovery mechanism in unconsolidated sand reservoirs. Extensive research is currently being conducted by universities and industry in the U.S. and Canada to improve CHOPS technologies and increase heavy oil recovery.

2.1.3 Oil Sands. In contrast to the very limited development of oil shale in the U. S., oil or tar sands in Canada are extensively produced. Oil sands are extremely limited in the U.S. with no commercially viable deposits. However, in Canada, particularly in Alberta and British Columbia, oil sand deposits are vast and have contributed significantly to the economy. Oil from oil sands has kept Canada as one to top exporters of oil to the United States in recent years. Canadian oil sands deposits are very shallow and are surface mined and refined on-site. Because of the complex retorting and refinery processes required, oil sands are more expensive to produce than conventional oil resources. The volume of oil sand resources and the speed of development has resulted in challenges with infrastructure, pipelines and manpower shortages attempting to keep with up with production.

2.1.4 Shale Gas Plays. The unconventional resource that is capable of providing significant volumes of natural gas to enhance America's economy is shale gas (Figure 2.5). The natural gas content of certain shale has been known for some time, but it has only been in the past ten years that shale gas development has boomed. Estimates have

been made that predict that by the end of 2035 about 46% of all natural gas produced in the U.S. will come from shale gas resource plays (Figure 2.6). Resource plays as contrasted with exploration plays have a low geologic risk of not finding gas, but the potential profits per well are generally lower. However, the total potential profits are very good considering the large amount of reserves.

Figure 2.5 North America shale plays (EIA, Annual Energy Outlook 2011)

Resource plays are developed in specific basins and formations, which were previously bypassed as uneconomic or considered as sealing formations for conventional oil and gas reservoirs. These shale formations are tight reservoirs with low matrix

permeability and must be fractured to permit gas to flow. The first shale gas play to realize its potential was the Barnett Shale located in the Bend Arch-Fort Worth basins of north Texas. The Barnett is estimated to have over 30 trillion cubic feet (Tcf) of resource. The technologies which unlocked shale gas in the Barnett are a combination of hydraulic fracturing and horizontal drilling. Development of the Barnett began in the mid 1990s, and has expanded to cover large areas in the Fort Worth Basin including development under the city of Fort Worth. In the period from 2005-2007 drilling in the Barnett shale had a success rate of 100%.

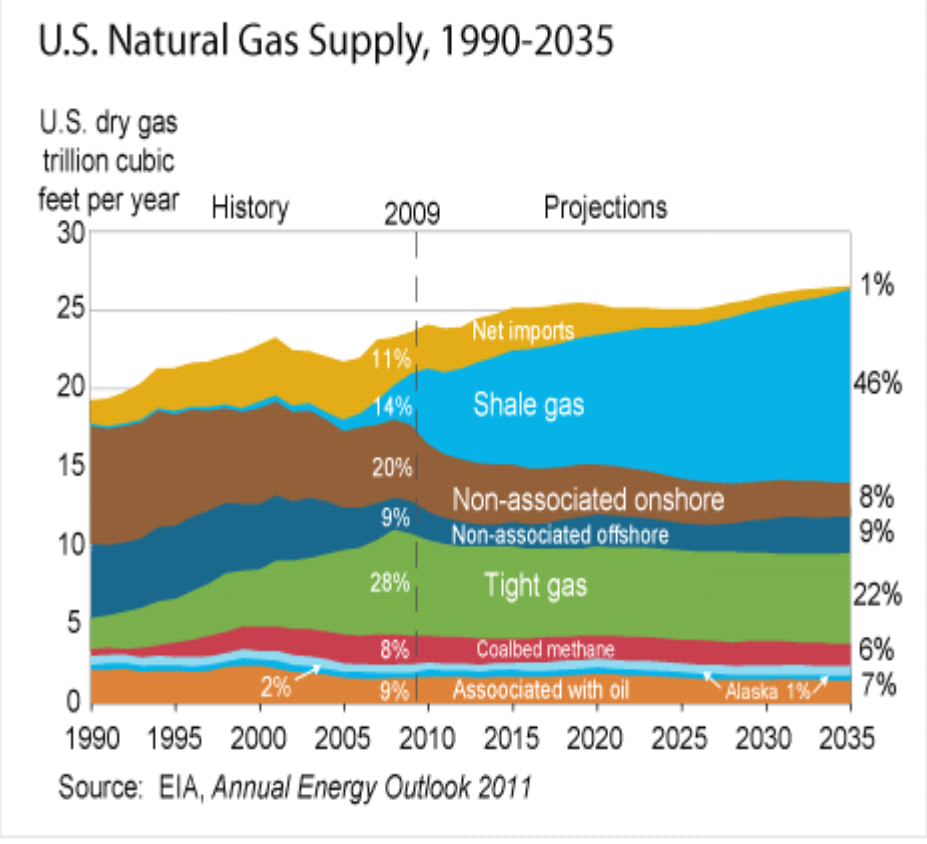

Figure 2.6 Current and estimated natural gas supply from 1990 to 2035 (EIA, Annual Energy Outlook 2011)

Current methods of producing shale gas depend on multi-stage hydraulic fracturing or hydrofracs in horizontal wellbores. Individual wells may require from 5 to 12 or more hydrofrac stages and the horizontal length may extend up to 10,000 ft. The hydrofracs require large volumes of fresh water, ranging from 2 to 10 million gallons per well. One of the important characteristics of shale gas plays is the degree of brittleness in the shale.

Shale with the desired degree of brittleness can be artificially fractured to create induced permeability which allows gas to flow. Since the distance a single hydraulically induced fracture can extend is limited, multi-stage fractures are required throughout the length of the horizontal borehole to access the maximum formation surface. Some shale is too plastic or ductile to allow hydrofracing and can't accommodate induced fractures to increase permeability.

Since 2007 the focus of shale gas production has shifted from exploration to economic management of water resources necessary for hydrofracing. Because of the large volumes of water required to hydrofrac individual wells, the withdrawal from surface water and aquifers has taxed the water resource availability in many areas. Shale gas operators find themselves in competition with agriculture, municipalities and other industries for water. In addition some 40% or more of the slick water is returned to the surface as frac-flowback water, requiring disposal. An entire research and service industry has developed around the shale gas industry to manage water handling issues. Traditional disposal methods relied primarily on reinjection wells, requiring massive transportation efforts.

The current research is targeting retreatment and beneficial use of the frac-flowback water including the technologies listed under CBM development. Beneficial uses include irrigation, livestock watering, municipal uses, fire control, and recycling for injection in new shale gas wells. Treatment technologies focusing on cleaning flowback water to levels required for recycling rather that attempting to meet potable water standards are of increasing interest. Regulatory issues at the federal, state and local level are a significant problem in some areas and shale gas operations have been suspended in some states pending decisions on proper water management procedures.

The U. S. Department of Energy has funded a number of research projects focused on evaluating treatment technologies, identifying best practices for individual plays or regions, and recycling of frac-flowback water.

2.1.5 Tight Oil Reservoirs. The most significant tight oil reservoir in the United States is the Bakken Shale Formation in the Williston Basin, with development in North and South Dakota, Montana, Saskatchewan and Manitoba. In April 2008 the United States Geological Survey (USGS) released results of a study on the Bakken Formation in North Dakota and Montana identifying 3 to 4.3 billion barrels of technically recoverable oil. This estimate was 25 times higher than the 1995 estimate of 151 million barrels. Technically recoverable oil resources are those producible using currently available technology and industry practices and the USGS is the only provider of publicly available estimates of undiscovered technically recoverable oil and gas resources. The reason for the new assessment of the Bakken was the phenomenal success that hydraulic fracturing

technology has made in producing from this tight oil shale play. New geological modeling and exploration techniques combined with advances in drilling and completion technologies have opened up the Bakken as the largest oil play in the Continental U.S. and the largest "continuous" oil accumulation ever assessed by the USGS. By the end of 2007 over 105 million barrels of oil had been recovered from the Bakken since discovery of the first Bakken oil field, Elm Coulee, in Montana in 2000. 65 million barrels have been produced from Elm Coulee alone.

The Bakken Formation is a relatively tight formation consisting of low porosity and permeability shale. Three members; a lower shale, a middle sandstone and an upper shale are Upper Devonian to Lower Mississippian in age. The organic rich shale members are the source rock for the Bakken and the overlying Mississippian Lodge pole Formation. Most of the undiscovered oil resides within a continuous composite reservoir that is distributed across the entire area of the oil generation window and includes all members of the Bakken Formation. To overcome poor fluid flow rates, wells are drilled horizontally, and then hydro-fractured to create open fractures, enhancing permeability in these tight rocks. The Bakken Formation ranges in depths from 8,000 ft to 11,000 in general getting shallower as you go eastward from Montana into North Dakota in the Williston Basin. Sweet spots in North Dakota in the Parshall and Sanish fields (discovered in 2006) have had impressive production rates with 25% of the wells producing over 3,000 BOEs/day.

2.1.6 Oil Shale. Oil shale is a solid sedimentary rock high in kerogen. When heated in a chemical process, called pyrolysis oil shale releases petroleum liquids. The vast potential for recovery of oil from oil shale deposits in Colorado, Utah and Wyoming has been recognized since the late 1970s. The Green River Formation contains the largest oil shale deposits in the world, with an estimated resource of 1.2 to 1.8 trillion barrels of oil equivalent. A moderate estimate of recoverable oil shale reserves is 800 million barrels from the Green River Shale. This volume is three times the proven oil reserves of Saudi Arabia. The majority of oil shale resources in the U.S. are on federally controlled lands.

Historically the cost of producing oil shale has been much higher than the cost of producing conventional oil, and technologies have lagged. High oil prices in the 1970s, 1980 and 2008 have periodically renewed the interest in developing economically feasible oil shale technologies. Traditional oil shale recovery involves underground mining using the room-and-pillar method or surface mining. After mining, the oil shale is transported to a facility for retorting, a heating process that separates the oil fractions of oil shale from the mineral fraction. After retorting, the oil must be upgraded by further processing before it can be sent to a refinery.

Recently Shell conducted pilot demonstrations in Colorado of in-situ recovery. The process involves heating underground oil shale, using electric heaters placed in deep vertical holes drilled through a section of oil shale. The oil shale is heated over a period of two to three years, until it reaches 650–700°F, at which point oil is released from the shale and collected in wells positioned within the heated zone. The perimeter of the zone

is surrounded by a barrier or freeze wall consisting of boreholes through which a refrigeration fluid is pumped. The freeze wall prevents groundwater from entering the production zone, and other fluids or contaminants from leaving the zone and entering the groundwater.

However, both mining and surface retort production and in-situ production methods have proved to be very high cost and take a high toll on environmental resources. Various environmental, state and local groups have opposed oil shale production on the grounds of damage to the environment through surface mining, transportation issues, water usage and air pollution. Both mining and retorting and in-situ recovery require large amounts of water and energy which could severely strain the land resources of the region. As the majority of oil shale resources are on Federal land, the Department of the Interior has severely restricted development.

2.1.7 Estimated Total Reserves. According to the latest estimation technique shifts assessment of global unconventional gas resources (Simon Chipperfield, 2012), the assessment of regional unconventional gas and conventional hydrocarbons (oil plus gas) in place indicates that 83,400 Tcf – 184,200 Tcf of unconventional gas and 58,300 Tcf –181,700 of conventional hydrocarbons exist worldwide. The estimated us reserves is updated to 750 Tcf shale gas and 24 BBO shale oil (US Department of Energy, 2011).

J.A. Masters suggested in a 1979 paper that hydrocarbon resource types can be assigned to various resources classes in a triangular distribution and that their positions in the triangle reflect their abundance, their reservoir quality, and the technology required

for recovery (Figure 2.7). As one goes lower on the gas resource triangle, the reservoirs are lower grade, which usually means the reservoir permeability is decreasing. These low-permeability reservoirs are much larger than the higher-quality reservoirs.

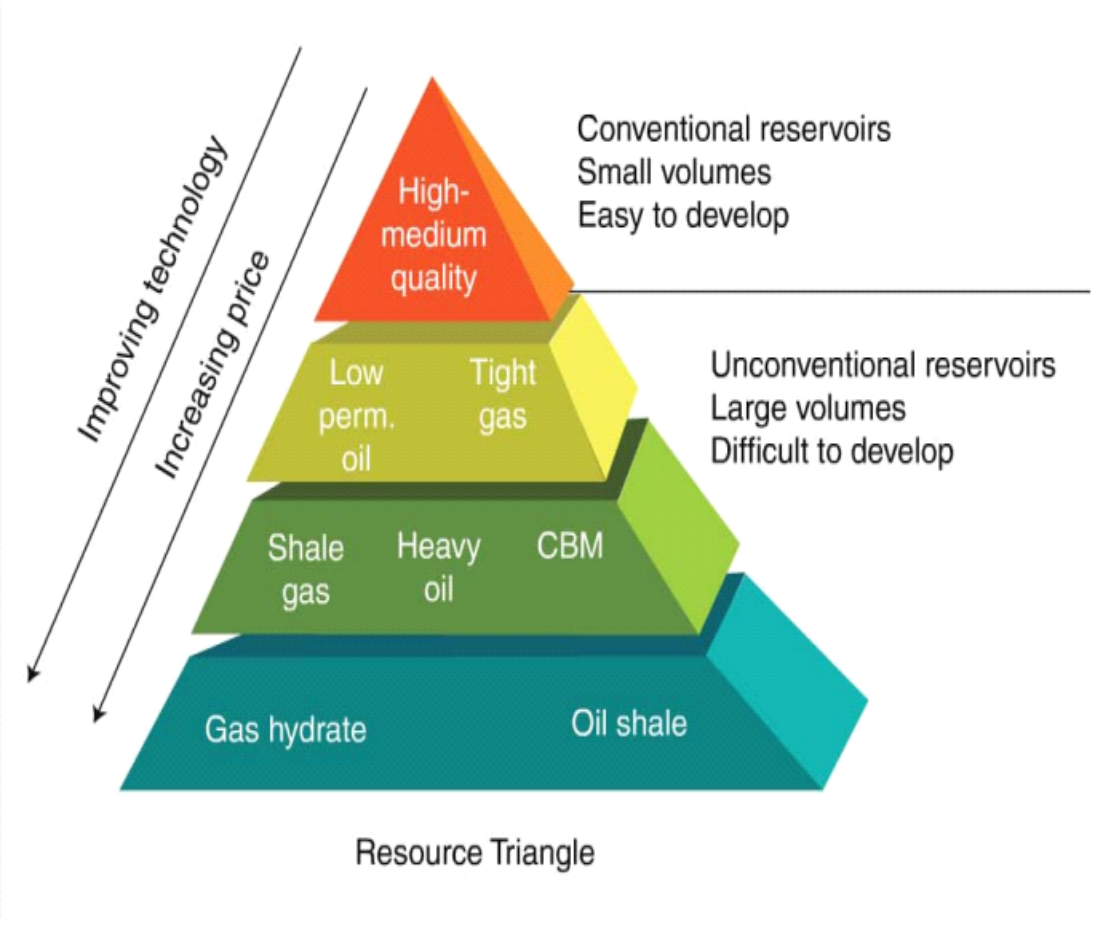

Figure 2.7 J.A. Masters' resource triangle (Simon Chipperfield, 2012)

2.2 PERMEABILITY AND RESERVOIR DESCRIPTION

Permeability is one of the most important concepts in determining the flow characteristics of hydrocarbons in oil and gas reservoirs, and of groundwater in aquifers.

Along with porosity, wettability and fluid viscosity we can better describe a reservoir's reserves and recover difficulty. The concept of permeability basically describes the ability for a fluid to transport through a porous media. The measure and obtain of permeability differs between gas and liquid, one phase and multi-phase.

2.2.1 Absolute Permeability. The generalized concept of permeability refers to absolute permeability, which states that the permeability value in question is an intensive property (not a spatial average of a heterogeneous block of material), that it is a function of the material structure only and not of the fluid.

Permeability is part of the proportionality constant in Darcy's law which relates discharge (flow rate) and fluid physical properties (e.g. viscosity), to a pressure gradient applied to the porous media:

$$k = \frac{v\mu\Delta x}{\Delta P}$$

where v is the superficial fluid flow velocity through the medium (m/s), k is the permeability of a medium (m^2), μ is the dynamic viscosity of the fluid (Pa·s), ΔP is the applied pressure difference (Pa), Δx is the thickness of the bed of the porous medium (m).

In naturally occurring materials, permeability values range over many orders of magnitude. The concept of absolute permeability explicitly distinguishes the value from that of relative permeability.

2.2.2 Relative Permeability. Relative permeability indicates a dimensionless measure of the effective permeability of one phase In multiphase flow in porous media. It

can be viewed as an adaptation of Darcy's law to multiphase flow. For two-phase flow in porous media given steady-state conditions, we can write

$$q_i = -\frac{k_i}{\mu_i}\Delta P \qquad \text{for } i = 1, 2$$

where q_i is the flux, ΔP is the pressure drop, μ_i is the viscosity, k_i is here the phase permeability, as observed through the equation above.

Relative permeability, k_{ri} for phase i is then defined as $k_i = k_{ri}k$, $k_{ri} = \frac{k_i}{k}$ where k is the permeability of the porous medium in single-phase flow which also means the absolute permeability. Relative permeability must be between zero and one.

In applications, relative permeability is often represented as a function of water saturation, however due to capillary hysteresis, one often resorts to one function or curve measured under drainage and one measured under imbibition.

Under this approach, the flow of each phase is inhibited by the presence of the other phases. Thus the sum of relative permeability over all phases is less than 1. However, apparent relative permeability larger than 1 have been obtained since the Darcean approach disregards the viscous coupling effects derived from momentum transfer between the phases. This coupling could enhance the flow instead of inhibit it. This has been observed in heavy oil petroleum reservoirs when the gas phase flows as bubbles.

2.2.3 Permeability of Gas. Sometimes permeability to gases can be somewhat different from those for liquids in the same media. One difference is attributable to "slippage" of gas at the interface with the solid (L. J. Klinkenberg, 1941) when the gas mean free path is comparable to the pore size.

Under steady state and laminar flow condition, Klinkenberg demonstrated that the permeability to gases is approximately a linear function of the reciprocal pressure. When Klinkenberg defined the interactions to be considered, he supposed the existence of a layer, thinner than molecular mean free path, adjacent to the pore's wall where only molecules-wall collisions would occur and collisions among molecules could be ignored. Thus the slippage velocity, as obtained from the Klinkenberg's approach, captures the contribution of molecule-wall interactions and when this velocity is zero, the Poiseuille velocity profile is recovered. However, Klinkenberg's formulation ignores the transition flow region, where neither molecule-molecule nor molecule-wall interactions can be neglected because both are playing a relevant role. The feasibility of Klinkenberg linear function of the reciprocal pressure depends on the Knudsen number. For Knudsen numbers from 0.01 to 0.1 the Klinkenberg approach is acceptable.

For those diffusion that Knudsen numbers are larger than 1, consider the diffusion of gas molecules through very small capillary pores. If the pore diameter is smaller than the mean free path of the diffusing gas molecules and the density of the gas is low, the gas molecules collide with the pore walls more frequently than with each other. This process is known as Knudsen flow or Knudsen diffusion.

The Knudsen number is a good measure of the relative importance of Knudsen diffusion. A Knudsen number much greater than one indicates Knudsen diffusion is important. In practice, Knudsen diffusion applies only to gases because the mean free path for molecules in the liquid state is very small, typically near the diameter of the

molecule itself. The diffusivity for Knudsen diffusion is obtained from the self-diffusion coefficient derived from the kinetic theory of gases.

The Knudsen number is a dimensionless number defined as:

$$\mathrm{Kn} = \frac{\lambda}{\mathrm{L}}$$

where λ is mean free path, L is representative physical length scale. For an ideal gas, the mean free path may be readily calculated so that:

$$\mathrm{Kn} = \frac{k_B T}{\sqrt{2}\pi\sigma^2 pL}$$

where K_B is the Boltzmann constant (1.3806504(24) × 10−23 J/K in SI units), T is the thermodynamic temperature, σ is the particle hard shell diameter, and p is the total pressure.

Gas permeability of reservoir rock and source rock is important in petroleum engineering, when considering the optimal extraction of shale gas or tight gas.

2.3 CURRENT LAB METHODS FOR MEASURING PERMEABILITY

Gas permeability needs to be measured. Normally when pore size is larger than nano-level we can directly using Darcy's law and Klinkenberg correction to calculate. As long as pore size reaches nano-level, Knudsen diffusion start to occur and permeability should be calculated through estimation using empirically derived formulas.

However, for some simple models of porous media, permeability can be calculated. According to the different shape, pore size and other characteristics of studied porous

media, different methods were developed for measuring pressure difference and flow rate in lab.

2.3.1 Core Holder. As the most common method for use in testing of a geologic core sample or other similar cylindrical sample, core holders are generally used for measuring gas or liquid flow in certain cores of geological formation. More particularly, to such a core holder with means for simultaneously subjecting such a sample to axial and radial pressures of unequal magnitude and the capability of being contained in a conventional laboratory oven during testing to simulate in situ conditions of the formation from which the core was taken.

It is common practice in the petroleum industry to remove core samples from sub surface geologic formations for testing. Typically, a core barrel is used to remove cores at intervals as a well is drilled. Some core samples are used for routine tests of the porosity, permeability and other important characteristics of a petroleum producing formation. Other core samples are used for water flooding, enhanced recovery, formation damage or other special tests.

It is usually desirable for both routine and special tests of core samples to be conducted at pressures simulating those encountered in the subsurface geologic formations from which the core samples were removed. Usually, such tests are conducted at room temperature. However, t is sometimes desirable for such tests to be conducted at temperature greater than room temperature. Accordingly, it is desirable to have core holders which permit such tests to be conducted at various pressures within a range of

pressures greater than atmospheric pressure and temperatures greater than room temperature.

A core holder is desirable with means for simultaneously subjecting a core sample to axial and radial pressures of unequal magnitude which is capable of being contained in a conventional laboratory oven during testing. It is also desirable to have such a core holder which can accommodate a varying number of fluid supply lines, electrical wires and the like necessary for various routine and special tests. It is not believed that the prior art provides such a core holder.

2.3.2 Pulse-decay Technique. The pulse-decay apparatus, shown schematically in Figure 2.8, consists of an upstream reservoir of volume V_u, a downstream reservoir of volume V_d, and a cell capable of applying hydrostatic comfining pressure (P_c) and containing a cylindrical rock sample with a total pore volume V_p. A differential pressure transducer measures the pressure difference (ΔP) between the reservoirs and a second transducer measures the absolute pressure (P_d) in the downstream reservoir. The absolute pressure in the upstream reservoir can be measured by another transducer or calculated from P_d and ΔP.

A typical pulse-decay measurement for low-permeability rocks is conducted with the following procedure. Starting with valves 1, 2, and 3 open to avoid gas-slippage (Klinkenberg) effects, high-pressure gas is injected into the sample and the upstream and downstream reservoirs. When the pressure equilibrates throughout the entire system at P_{d0}, valves 2 and 3 are closed. Next, the pressure in the upstream reservoir is increased by

a few percent (e.g. 5%) of P_{d0}. Once the gas in the upstream reservoir re-achieves equilibrium, valve 2 is opened and the gas flow through the sample with a 'pressure pulse'. The pressure difference (ΔP) across the sample is monitored with time. The ΔP-t data series can then be analyzed to determine the sample permeability based on an analytical solution of the equations describing the pressure change during the experiment with known parameters of reservoir volumes, sample pore volume, and gas properties (e.g. viscosity).

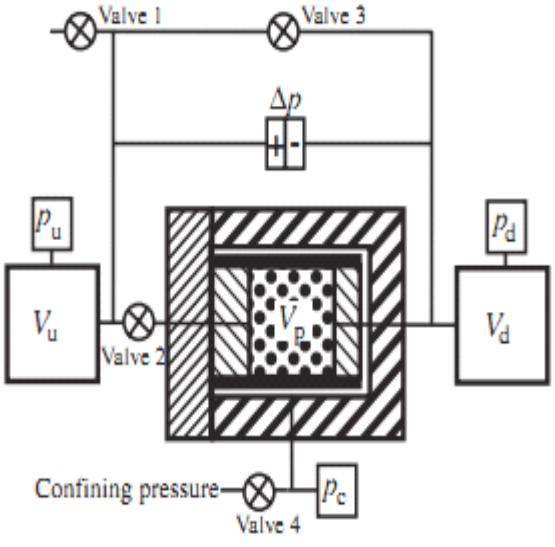

Figure 2.8 Modified pulse decay apparatus for low permeability media (S.C. Jones, 1997)

The dimensionless differential pressure (ΔP_D) between the upstream and downstream reservoirs is defined as:

$$\Delta P_D = \frac{P_u(t) - P_d(t)}{P_u(0) - P_d(0)}$$

If the experiment only involves very small pressure changes (i.e. <5%), then the experimental dimensionless differential pressure at larger time becomes a single exponential function of time and can be approximated as (Dicker & Smits 1988; Jones 1997):

$$\ln(\Delta P_D) = \ln(f_0) + s_1 t$$

where f_0 is a constant and s_1 is:

$$s_1 = -\frac{kf_1 A\left(\frac{1}{V_u} + \frac{1}{V_d}\right)}{\mu L c_g}$$

where $f_1 = \theta_1^2/a+b$, θ_1 is the first solution of the transcendental equation:

$$\tan\theta = \frac{(a+b)\theta}{\theta^2 - ab}$$

and a and b are gas-storage capacity ratios of sample to upstream and downstream reservoirs, respectively, as defined by

$$a = \frac{V_p(1+f_a)}{V_u} \text{ and } b = \frac{V_p(1+f_a)}{V_d}$$

If no adsorption occurs, f_a becomes zero and a and b become the same ratios defined in previous studies (Dicker& Smits 1988; Jones 1997).

With experimental pulse-decay data, ΔP_D can be calculated and plotted logarithmically versus time to obtain a straight line for late-time (or large-time) data and the slope, s_1, can be obtained by linear curve fitting. Then, the permeability of the sample can be determined with simple manipulation of equation as follows:

$$k = \frac{-s_1 \mu L c_g}{f_1 A(1/V_u + 1/V_d)}$$

2.3.3 Crushed Samples. Reservoir rocks are routinely crushed to small particle sizes to determine their skeleton density or porosity using He expansion, or to determine adsorption isotherms for various gases using pycnometry with gas expansion. The pressure decay with time after gas expansion begins can be utilized to determine gas permeability (e.g. Luffel et al. 1993; ResTech 1996; Egermann et al. 2005).

A schematic diagram of a typical pycnometer is shown in Figure 2.9. The pycnometer consists of two cells, the reference cell (volume V_r) and sample cell (volume V_s), a series of valves, and high-precision transducers. In order to measure porosity or skeleton density of reservoir rocks using gas (commonly He), rocks are first crushed into small particles and then put into the sample cell. Valve 2 is then closed, valve 3 is turned on, the sample is flushed using the experimental gas, and then the sample cell is vacuumed to remove air. After that, valve 3 is closed and the pressure in the sample cell (P_0) is recorded. High pressure gas is then loaded into the reference cell by turning valve 1 on and then off. After some time, gas in the reference cell reaches equilibrium and its pressure (P_{r0}) is recorded. Then, valve 2 is opened and the high pressure gas in the reference cell is allowed to expand into the sample cell. The pressures in either the reference or sample cells or both are monitored. Gas pressure in the reference cell will immediately drop as gas occupies the void volume in the sample cell. Thereafter, the pressure will continuously decrease, as gas penetrates into crushed porous particles until equilibrium is reached with a final equilibrium pressure (P_e).

With known sample mass (M) and bulk density (ρ_b) measured independently by Hg intrusion, the sample skeleton density (ρ_s) and porosity (φ) can be determined as follows, provided no adsorption occurs as when it is applied:

$$\Phi = \left[V_t\left(\frac{p_{r0}}{z_{ro}} - \frac{p_c}{z_c}\right) + (V_s - V_b)\left(\frac{p_0}{z_0} - \frac{p_c}{z_c}\right)\right] / \left(\frac{p_c}{z_c} - \frac{p_0}{z_0}\right)V_b$$

where V_b is the bulk volume of the sample (including the pore space), given as M/ρ_b, and z is the gas compressibility factor at different pressures.

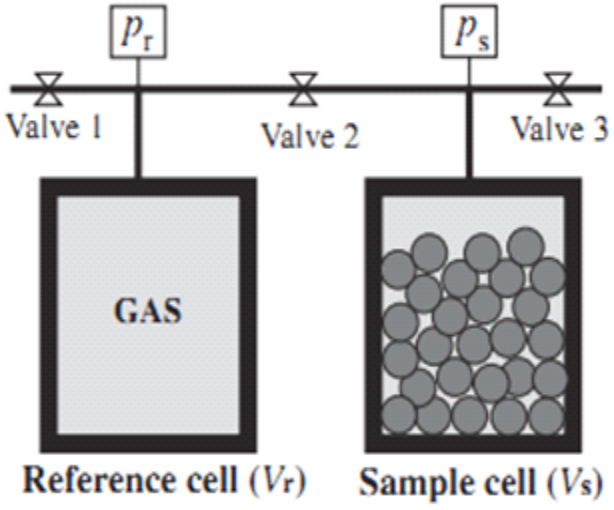

Figure 2.9 Pycnometer model for Crushed samples, (X. Cui, 2009)

During a dynamic pycnometer experiment, the mass fraction (F_R) of gas in the void volume of the reference and sample cells that will eventually be taken up by the sample particles relative to the total gas that can be taken by the sample can be calculated from experimental data as:

$$F_R = 1 - \frac{(K_c + 1)(\rho_{c0} - \rho)}{(\rho_{c0} - \rho_0)}$$

where K_c is the ratio of the gas storage capacity of the total void volume of the reference and sample cells (V_c) to the total void volume of the sample particles and is given as:

$$K_c = \frac{\rho_b V_c}{M[\Phi + (1-\Phi)K_a]}$$

and ρ_{c0} is the average initial gas density in the sample and reference cell, given as:

$$\rho_{c0} = \frac{\rho_{r0} V_t + \rho_0 (V_s - V_b)}{V_t + V_s - V_b}$$

If the particles can be approximated as spheres with a relatively uniform radius (R_a) and the pressure change during the experiment is relatively small, then the residual gas fraction (F_R) is theoretically given as:

$$F_R = 6K_c(K_c+1)\sum_{n=1}^{\infty} c^{-K\alpha_n^2 t/R_L^2} \frac{1}{K_c^2\alpha_n^2 + 9(K_c+1)}$$

where K is the apparent transport coefficient as defined in equation above and α_n is the nth root of

$$\tan\alpha = \frac{3\alpha}{3 + K_c\alpha^2}$$

If the total void volume of the reference and sample cells is much larger than the total gas-storage capacity of the sample particles (i.e. $K_c \propto \infty$), such that the pressure in the reference or sample cells will remain nearly constant, thus the gas residual ratio becomes:

$$F_R = \frac{6}{\pi}\sum_{n=1}^{\infty} e^{-\pi^2 n^2 Kt/R_L^2} \frac{1}{n^2}$$

This equation is widely encountered in literature, but it is just an end-member case of the more general solution.

2.3.4 Canister Desorption Test. Drill cores are often desorbed on site to evaluate the gas content of target gas-shale reservoirs and often provide the only information available to evaluate permeability and/or diffusion in gas shales and coal. Because of the nature of the samples and measurements (outlined below), the permeabilities derived from desorption tests are not as accurate as those obtained by other methods. The desorption data do, however, allow quantitative assessment of permeability and diffusivity, and thus we provide the theoretical bases for analyses with the recognized caveat that the nature of the samples has a significant bearing on the utility of the results. There are many kinds of instruments for desorption tests, but in principle they are similar to the Inverted Cylinder (USBM System) as sketched schematically in Figure 2.10.

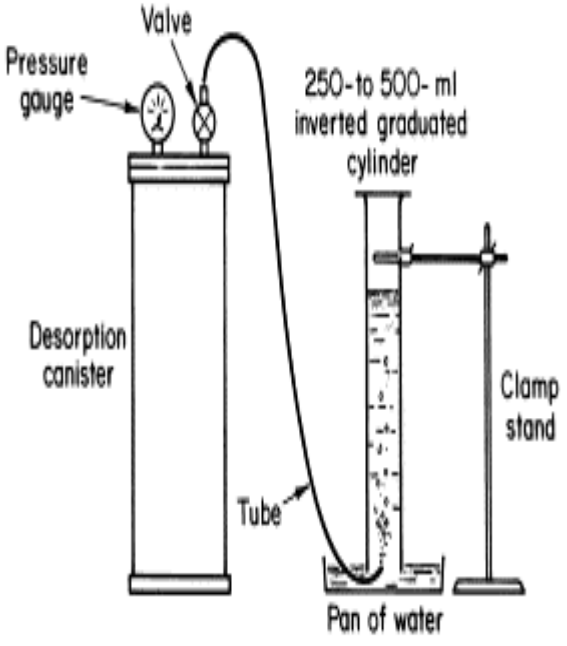

Figure 2.10 Schematic sketch of a desorption-test apparatus (P.D. William, 1998)

The cumulative volume of released gas is measured with time. If the length of the core that is being desorbed is much larger than its diameter, the fraction of cumulatively desorbed gas relative to the total gas to be desorbed (F_D) can be approximated analytically by assuming one-dimensional radial flow out of an infinitely long cylinder.

The late-time desorbed gas fraction (F_D) can be fitted by

$$\ln(1 - F_D) = f_0 - s_1 t$$

and the permeability can be determined with the late-time data as:

$$k = \frac{R_a^2[\Phi + (1 - \Phi)]\mu c_g s_1}{\xi_1^2}$$

where ξ_1 is the first root of the Bessel equation $J_0(\xi) = 0$ and is equal to 2.404834, and the other parameters remain the same as those defined in previous sections. At early time, the gas desorption fraction (F_D) is approximately a linear function of the square root of time and can be fitted with:

$$F_D = s_0\sqrt{t}$$

The permeability can then be determined with the early time data as:

$$k = \frac{\pi R_a^2[\Phi + (1 - \Phi)]\mu c_g s_0^2}{16}$$

2.4 FLUID FLOW MODELS CONSIDERING KNUDSEN DIFFUSION

2.4.1 Florence Fluid Diffusion Model. F.A. Florence derived a fluid diffusion model based on Klinkenberg effect (Klinkenberg, 1941) and also Jones Owens (F.O. Jones et al., 1979) and Sampath-Keighin (K. Sampath, 1981) correlations.

According to Florence, a rigorous microflow model for gas flow in an Idealized porous medium can be derived as follows:

Karniadakis and Beskok developed a unified model that predicts volumetric and mass flow rates for gas flow in channels and pipes over the entire Knudsen regime (i.e., all flow regimes). The Karniadakis-Beskok "microflow" model is given (without derivation) as:

$$q = \frac{\pi}{8} l_{char}^4 \frac{l}{\mu} \frac{\Delta p}{L} [1 + \alpha(K_n)K_n][1 + \frac{4K_n}{1 - bK_n}]$$

Where:

q = volumetric flow rate in the conduit with cc/sec

l_{char} = Characteristic length of the flow geometry (e.g., channel height, pipe radius), cm

L = Length of conduit, cm

ΔP= Pressure drop across the length of the conduit, atm

μ = Gas viscosity at temperature and pressure, cp

b = Dimensionless slip coefficient, (b is defined as -1)

α(Kn) = Dimensionless term in the rarefaction coefficient

Poiseuille's law for fluid flow in a pipe (or tube) is given by:

$$q = \frac{\pi}{8} l_{char}^4 \frac{l}{\mu} \frac{\Delta p}{L}$$

while Darcy's law for fluid flow in a porous media is:

$$q = kA_{core} \frac{l}{\mu} \frac{\Delta p}{L}$$

From above equation, A is the cross-sectional area of the porous medium (perpendicular to the direction of the flow). Following the procedure given by

Klinkenberg, equate Poiseuille's and Darcy's laws to yield an expression for the permeability (k), which yields:

$$k = \frac{\pi}{8}\frac{l_{char}^4}{A_{core}}$$

Substituting the equation into Karniadakis-Beskok "microflow" model, have:

$$q = \frac{k}{\mu}A_{core}\frac{\Delta p}{L}[1 + \alpha(K_n)K_n][1 + \frac{4K_n}{1 - bK_n}]$$

Multiplying by $\frac{\mu}{A} * \frac{L}{\Delta P}$ and using b=-1, obtain:

$$q\frac{\mu}{A}\frac{L}{\Delta p} = k_\infty[1 + \alpha(K_n)K_n][1 + \frac{4K_n}{1 + K_n}]$$

where the left-hand-side is simply the "gas" permeability (k_a) as defined by Darcy's law (i.e., the "uncorrected" permeability). Making this reduction, the permeability equation base form is presented as

$$k_a = k_\infty[1 + \alpha(K_n)K_n][1 + \frac{4K_n}{1 + K_n}]$$

The equation above provides an independent relation between the apparent gas permeability (k_a), the slip-corrected permeability (or Klinkenberg-corrected permeability) (k_∞), and the Knudsen number (Kn). We now need to finalize the equation by substitution of the relations for α(Kn). Substitute

$$\alpha(K_n) = \alpha_0\frac{2}{\pi}\tan^{-1}[c_1K_n^{c2}]$$

into Karniadakis-Beskok "microflow" model and assume that $c_1 = 4.0$ and $c_2 = 0.4$, which yields a direct relation for α(Kn) of the form of:

$$\alpha(K_n) = \frac{128}{15\pi^2}\tan^{-1}[4Kn^{0.4}]$$

Substituteα(Kn) into permeability equation base form to yield the result:

$$k_a = k_\infty \left[1 + [\frac{128}{15\pi^2}\tan^{-1}[4Kn^{0.4}]]K_n\right][1 + \frac{4K_n}{1+K_n}]$$

2.4.2 Javadpour Fluid Diffusion Model. Javadpour derived the gas flow model in nanopores from mass flux of a gas through a nanopore is the result of a combination of Knudsen diffusion and pressure forces, as presented in following equation:

$$J = J_a + J_D$$

where J is the total mass flux in $kg*s^{-1}*m^{-2}$. The first term on the right-hand side is advective flow due to pressure forces; the second term is Knudsen diffusion, as proposed by Javadpour for shale gas or mudrock systems.

$$J = U * \nabla c$$

$$J_D = -D_K : \nabla\nabla c$$

where U is average advective velocity in a pore and D_K is the Knudsen diffusion coefficient; c is concentration.

Roy et al showed that Knudsen diffusion in nanopores can be written in the form of pressure gradient. Gas mass flux by diffusion with negligible viscous effects in a nanopore is described as

$$J_D = \frac{MD_K}{10^3 RT}\nabla P$$

where M is molar mass, D_K is the Knudsen diffusion constant, R (= 8.314 J/mol/K) is the gas constant and T is absolute temperature in Kelvin. The Knudsen diffusion constant is defined as:

$$D_K = -\frac{2r}{3}(\frac{8RT}{\pi M})^{0.5}$$

Mass flux J_a for an ideal gas in laminar flow in a circular tube with negligible length of entrance effect can be derived from Hagen-Poiseuille's equation as:

$$J_a = -\frac{\rho r^2}{8\mu}\nabla P$$

Applying the ideal gas law to relate density to pressure, we can write:

$$J_a = -\frac{r^2}{8\mu}\frac{\rho_1}{p_1}p\nabla P$$

where ρ_1 and P_1 are density and pressure at the inlet of a pore, respectively. Integrating Equation over the length of the pore and defining $\rho_{avg} = 0.5*(\rho_1 + \rho_2)$ and $p_{avg} = 0.5*(p_1+p_2)$, in which subscript 2 denotes exit side of the pore, results in:

$$J_a = -\frac{r^2}{8\mu}\frac{\rho_{avg}}{L}\Delta P$$

where ρ_{avg} is in $kg*m^{-3}$. For very small pores at the nanoscale, the no-slip boundary condition is sometimes invalid. Brown et al introduced a theoretical dimensionless coefficient F to correct for slip velocity in tubes as:

$$F = 1 + \left(\frac{8\pi RT}{M}\right)^{0.5}\frac{\mu}{\rho_{avg}\, r}\left(\frac{2}{\alpha} - 1\right)$$

where p_{avg} is in Pa and α is the tangential momentum accommodation coefficient or, simply, the part of gas molecules reflected diffusely from the tube wall relative to specular reflection. The value of α varies theoretically in a range from 0 to 1, depending on wall surface smoothness, gas type, temperature and pressure. Experimental measurements are needed to determine α for specific mudrock systems.

Note that Brown's model was developed for extremely low pressure (vacuum) flow in large tubes. Whereas Javadpour's interest is in gas flow at higher pressures in nanopores, the governing physics is the same because the ratio of the mean free path of the gas to the tube (pore) diameter which defines the Knudsen number criterion for the slip flow regime, is in the same range for both systems.

The total mass flux through a nanopore by a combination of Knudsen diffusion and slip flow is:

$$J = -\left[\frac{2rM}{3 * 10^3 RT}\left(\frac{8RT}{\pi M}\right)^{0.5} + F\frac{r^2 \rho_{avg}}{8\mu}\right]\frac{(p_2 - p_1)}{L}$$

where gas constant R (= 8.314 J/mol/K) and r is the pore radius in m. Equation above shows that smaller pores result in higher values for multiplier F. Lower pressures also result in higher F.

From volumetric flux based on the Darcy equation

$$\frac{q}{A} = -\left(\frac{k_D \rho_{avg}}{\mu}\right)\frac{(p_2 - p_1)}{L}$$

where k_D is Darcy permeability, A is the cross-sectional area and L is the length of the media. This equation can be used for conventional systems, i.e., pore size range of tens to hundreds of μm. Similarly, volumetric gas flux Equation for nanopores is presented as:

$$\frac{q}{A} = -\left[\frac{2rM}{3 * 10^3 RT\rho_{avg}}\left(\frac{8RT}{\pi M}\right)^{0.5} + F\frac{r^2}{8\mu}\right]\frac{(p_2 - p_1)}{L}$$

where simplifies to the Darcy equation by increasing the size of pores or increasing pressure.

A new term called apparent permeability, k_{app}, for the gas flow in mudrock systems is obtained as

$$k_{app} = \frac{2r\mu M}{3 * 10^3 RT\rho_{avg}{}^2}\left(\frac{8RT}{\pi M}\right)^{0.5} + F\frac{r^2}{8\rho_{avg}}$$

Note that permeability in this system is not only a property of the rock system, but it also depends on properties of flowing gas at specified pressure and temperature. This dependence was expected from the beginning because interaction of different gases with the solid matrix is one of the parameters that was included in the model. Also, Knudsen diffusion, which is negligible for conventional systems, plays an important role in fine-grained mudrocks. One of the intriguing problems in the field of gas-producing mudrock strata is the higher than expected gas production from these reservoirs. To address this problem, we divided apparent permeability k_{app} by Darcy permeability k_D in equation:

$$\frac{k_{app}}{k_D} = \frac{2\mu M}{3 * 10^3 RT\rho_{avg}{}^2}\left(\frac{8RT}{\pi M}\right)^{0.5}\frac{8}{r} + [1 + \left(\frac{8RT}{M}\right)^{0.5}\frac{\mu}{\rho_{avg}{}^r}(\frac{2}{\alpha} - 1)]\frac{1}{\rho_{avg}}$$

The final equation suggests that the smaller the size of the pores, the larger the difference between apparent permeability and Darcy permeability. This equation also shows that the deviation between apparent permeability and Darcy permeability is larger at lower pressures. The contribution of Knudsen diffusion to total gas flow is larger at lower pressures.

3. METHODOLOGY

3.1 MEMBRANE CHARACTERIZATION

The ceramic membranes are round slices with thickness of 100μm and 25mm diameter. In order to have a better understanding of the materials, SEM figures were the last to be done but the first to be analyzed using SEM in Figure 3.1. SEM figures were taken for the membranes to give a precise value of pore diameter and pore density.

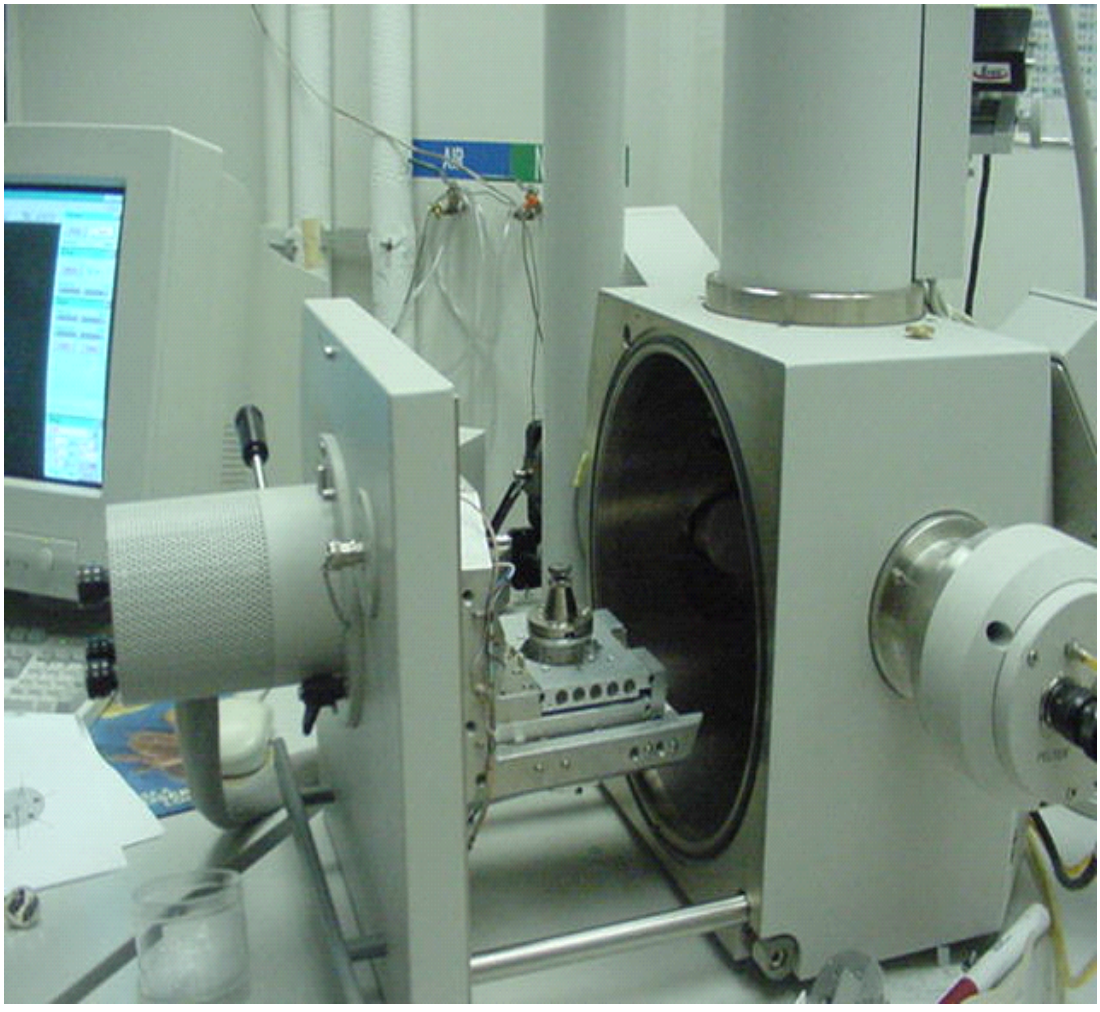

Figure 3.1 A scanning election microscope with opened sample chamber

A relatively panoramic view was taken first to show the membrane condition and check the uniformity of the membranes at first. Then by zooming in random places the, number of pores could be obtained which divided by area made pore density. The partial pores on the edges of the image were reading as 1/4, 1/2 and 3/4 pores. By continuous enlarging the magnification of the image till pore edges were clear, pore size was calculated through measuring scale which connected the edges proportion to magnification scale. Due to the unlevel of the membrane and shooting angle some pores were clearly not perpendicular to microscope lens which led to a diameter with visual error. Thus only the ones with regular shape and without vision of pore wall were measured can to be calculated into average pore size. SEM image example is showed in Figure 3.2.

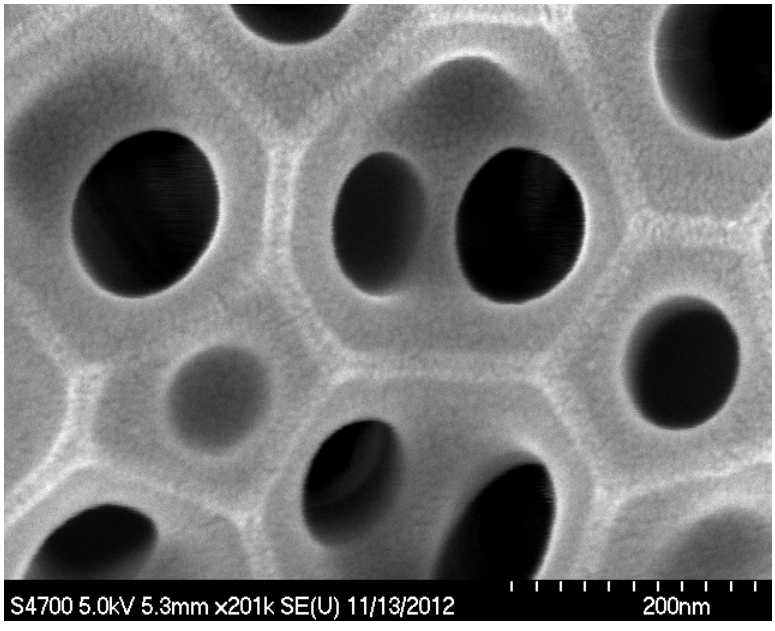

Figure 3.2 A SEM image for ceramic membrane

3.2 CORE FLOODING TEST USING GAS

Normally a shale or tight sample are measured by Pulse-decay methods or Canister Desorption Test for reasons of either long measuring time period due to extra low permeability or irregular shape and the demand of the confining pressure free measurement due to the low resistance to stress. Ceramic membranes avoid both features and can be measured using core flooding test with a relatively short time period as Figure 3.3 shows.

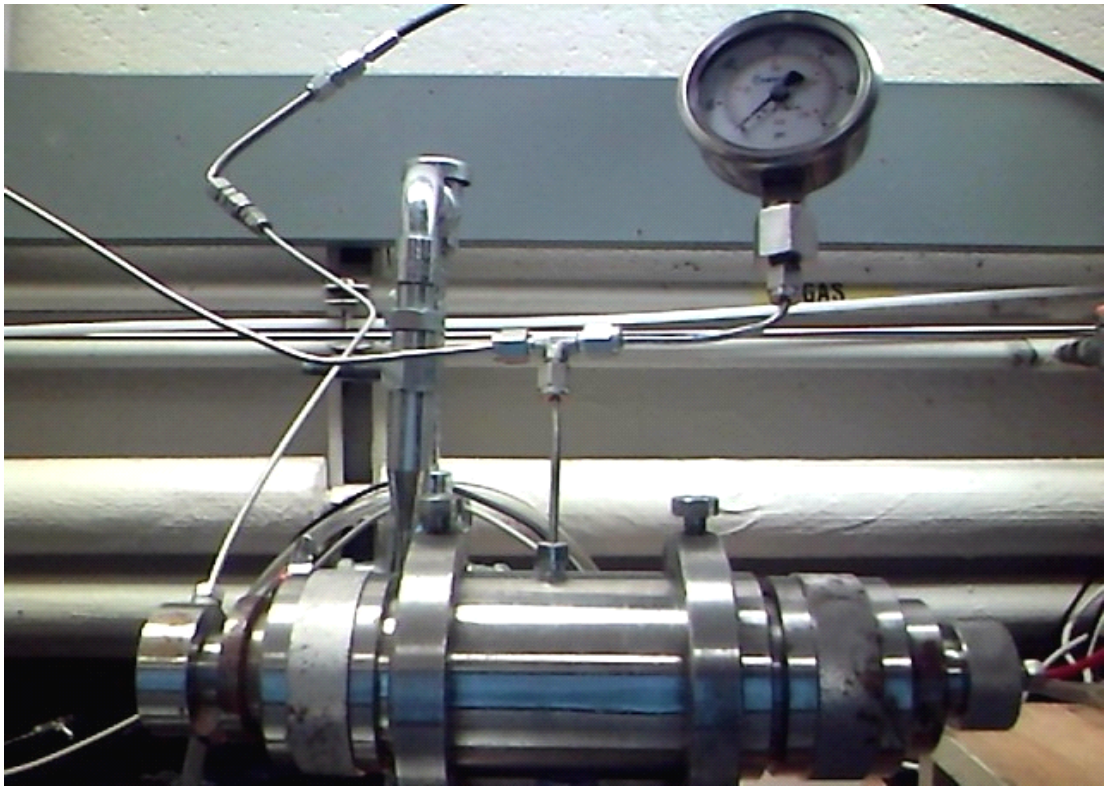

Figure 3.3 Core holder setup for gas injection

Ultra perm 600 was used to measure the pressure differences and flow rates. After added confining pressure, the core holder with the membrane inside was injected by gas

from upstream to downstream. Both upstream and downstream were measured by pressure meters and flow meters were set in downstream. By switching the upstream pressure to produce different pressure drops, the corresponding flow rate reading was recorded together to define the gas diffusion.

Membrane and other accessories inside the core holder is presented in Figure 3.4 in which from left to right the whole set up includes an aluminum cylinder, the membrane and an oring between the upstream and downstream parts.

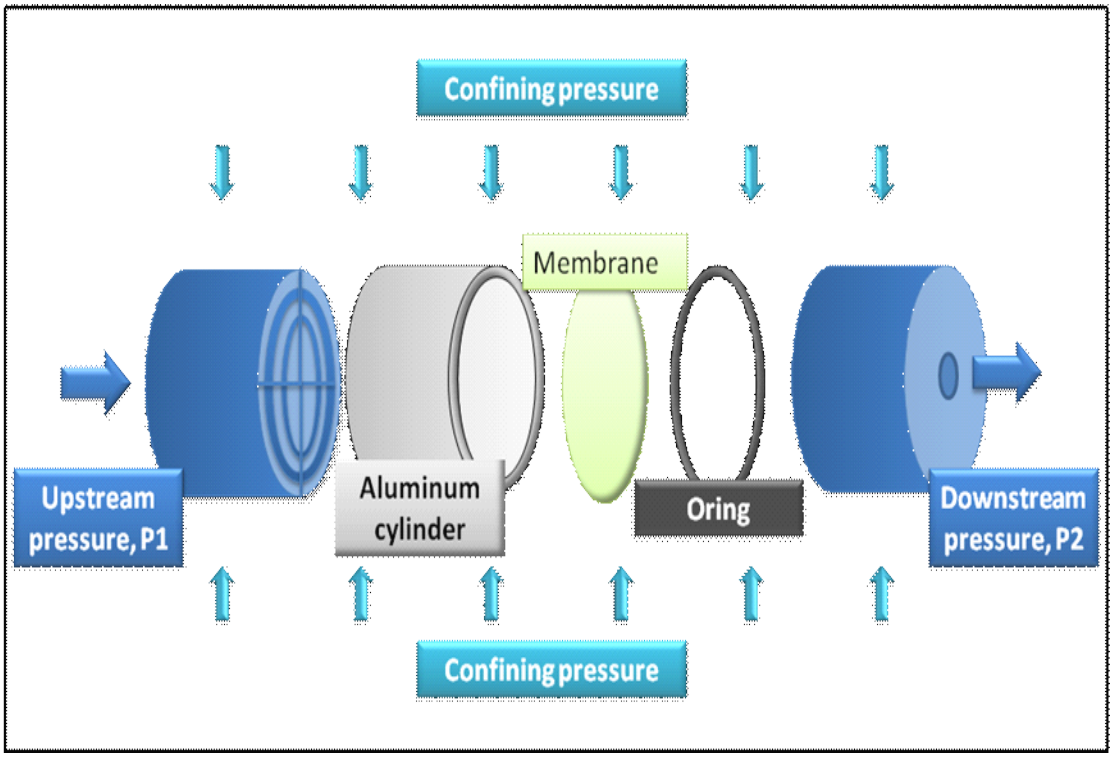

Figure 3.4 Components inside the core holder

The aluminum cylinder with a outer diameter of 25mm which exactly equals to the membrane diameter provides the necessary length demand for the core holder, the room

for a more even pressure on membrane and also a bolster to pretend the rubber cylinder which surrounds the membrane and provides the confining pressure from deformation and breaking the membrane. The rubber oring separates the membrane from the medal downstream part in case to serve a self pressure environment and to protect the membrane from contaminate by downstream part.

Pressure drop were taken from zero to dozens or even more the a hundred due to different pore distribution and accuracy of the flow meters. As for low permeability measurement, there is always a time period to reach the steady flow rate under certain pressure drop although the thickness of the membrane is relatively smaller. After pressure reached the highest value it was switched down and some extra flow rate point were measured to check for the repeatability.

3.3 CORE FLOODING TEST USING WATER

On the contrary to gas injection, flow rate is controlled to measure corresponding pressure in water injection. Different from gas injection, an accumulator was used to protect dirt or other particles entering core holder and plugging the membrane through de-ionized water. Except the accumulator, other setup including the components inside the core holder was same with that of gas measurement.

After getting the core holder saturated with de-ionized water, certain flow rate would be set for the injector and water would go into the accumulator in certain flow rate which

pushed the piston and made de-ionized water on the other side of piston enter core holder in the same flow rate. With the pressure meter recording pressures for upstream of the core holder and downstream opening to air, data would be collected by sensor and recorded by software as showed in Figure 3.5.

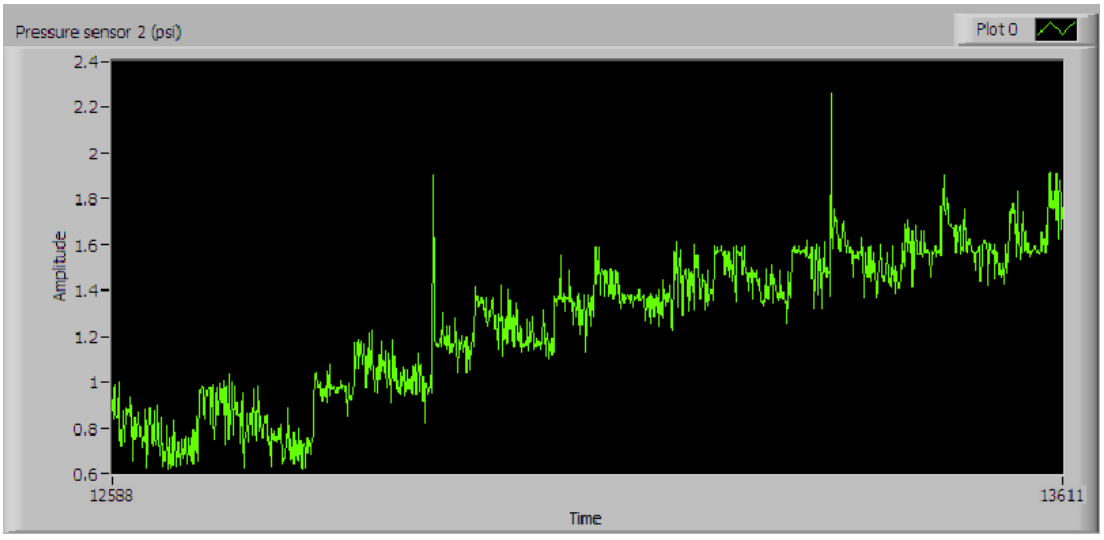

Figure 3.5 Pressure data recorded by sensor and software

4. MODEL USED FOR LAB DATA FITTING

4.1 DARCY'S LAW BASED KLINLENBURG CORRECTION

Darcy's law is a phenomenologically derived constitutive equation that describes the flow of a fluid through a porous medium. The law was formulated by Henry Darcy based on the results of experiments on the flow of water through beds of sand. (H. Darcy, 1856) Under steady state and laminar flow condition, Klinkenberg demonstrated that the permeability to gases is approximately a linear function of the reciprocal pressure. (Klinkenberg J.C., 1941)

Darcy's Law for gas flow, given in following equation:

$$\frac{1}{P_m} = \frac{2}{P_1 + P_2}$$

$$K_a = \frac{2000 \times L \times \mu \times P_m \times Q}{A \times (P_1^2 - P_2^2)}$$

4.2 KOZENY-CARMAN EQUATION

On account for the membranes are uniform and with known pore diameters and pore density. They can be considered as a bunch of nano-tube in parallel which simplify the porous model comparing to real core samples. The simplified equation of Kozeny-Carman equation might give a rough value of the permeability.

$$k = \frac{\Phi d_p^2}{32\tau}$$

4.3 FLORENCE'S NANO FLOW MODEL

The new microflow model represents gas flow in low permeability core samples and is also applied as a correlation for prediction of the equivalent liquid permeability in much the same fashion as the Klinkenberg model. The equation is derived to be:

$$k_a = k_\infty[1 + \alpha(K_n)K_n][1 + \frac{4K_n}{1 + K_n}]$$

In which

$$\alpha(K_n) = \frac{128}{15\pi^2}\tan^{-1}[4Kn^{0.4}]$$

4.4 JAVADPOUR'S NANO FLOW MODEL

The permeability in Javadpour model is not only a property of the rock system, but it also depends on properties of flowing gas at specified pressure and temperature. This dependence was expected from the beginning because interaction of different gases with the solid matrix is one of the parameters that was included in the model. Also, the model integrates Knudsen diffusion, which is negligible for conventional systems, plays an important role in unconventional reservoirs.

$$k_{app} = \frac{2r\mu M}{3 * 10^3 RT\rho_{avg}{}^2}\left(\frac{8RT}{\pi M}\right)^{0.5} + F\frac{r^2}{8\rho_{avg}}$$

In which

$$F = 1 + \left(\frac{8\pi RT}{M}\right)^{0.5}\frac{\mu}{\rho_{avg}{}^r}\left(\frac{2}{\alpha} - 1\right)$$

5. RESULTS AND DISCUSSIONS

5.1 SEM AND CALIBRATION OF MEMBRANES

To better determine the characteristics of the membranes, SEM pictures are taken for all the membranes. Figure 5.1 shows the crosssection of the membrane which demonstrates the nanomembranes have the tortuority equals to 1 and the sysmetric membrane model can be simiplified considered as a number of nanotube in parallel.

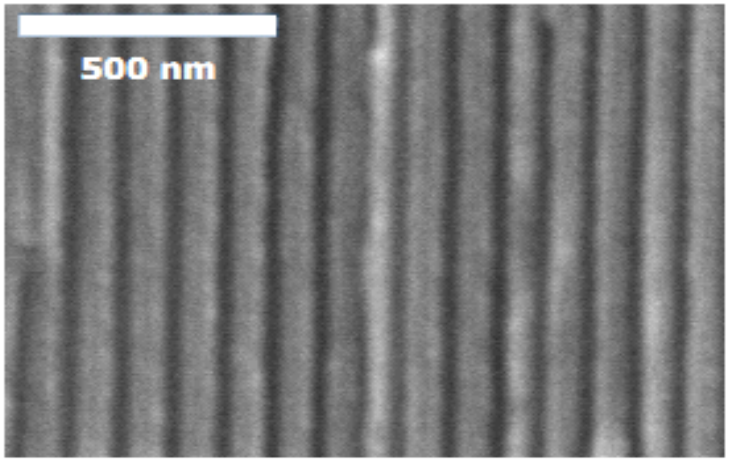

Figure 5.1 SEM of crosssection of ceramic membrane

Figure 5.2 indicates the conditions of 35nm membreane and two works have done to further describe and calibrate the pore density and pore size of the membranes. First, two random places were chosen to estimate pore density. Secondly, another two random pictures with larger magnification were used to calibrate the pore size of the membranes. All SEM pictures and calculation are as follows:

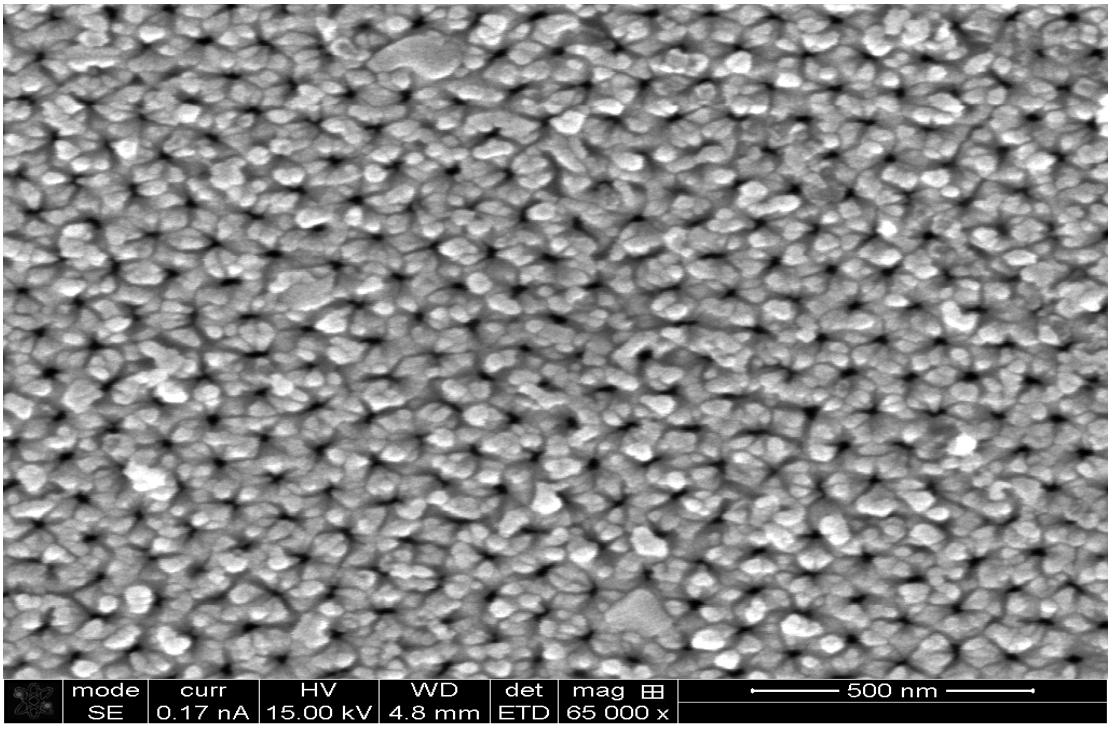

Figure 5.2 SEM of surface of 35nm membrane

For 35 nm membranes, Figure 5.3 shows the pore density of 33.5 pores/ 346951nm^2 and 32 pores/ 348644nm^2 respectively, thus the average pore density can be calculated as 9.42*10^{-5} pores/nm^2.

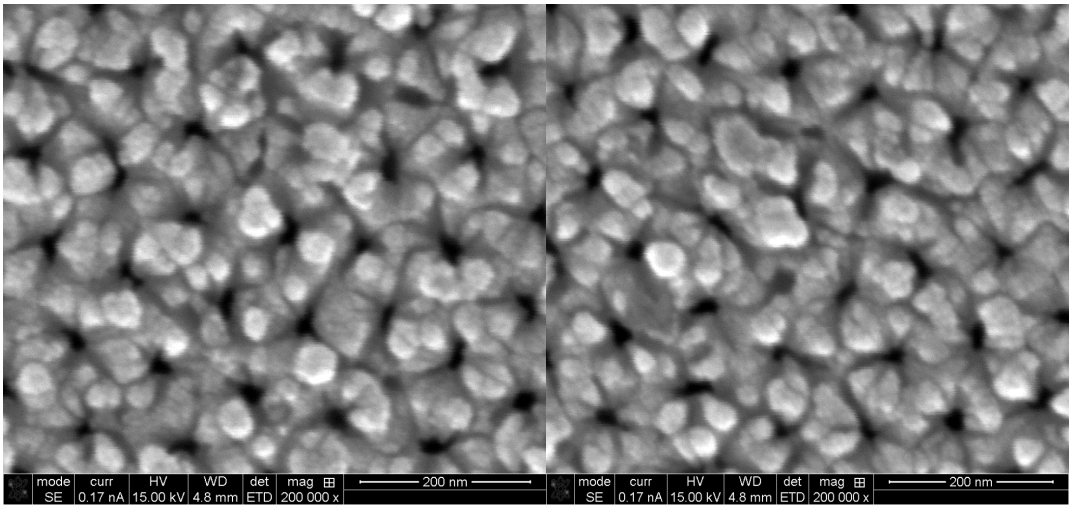

Figure 5.3 SEM figures randomly chosen to calculate pore density

As showed in Figure 5.4, pore diameter is measured according to the scale length. It is possible to have certain degree of oblique in such a small scale so that the relatively vertical pores are chosen to avoid measurement error. After the combination of Figure 5.4, the average pore diameter of the 35nm membranes is 19.8nm. Figure 5.5 shows the generally condition of 55nm membrane.

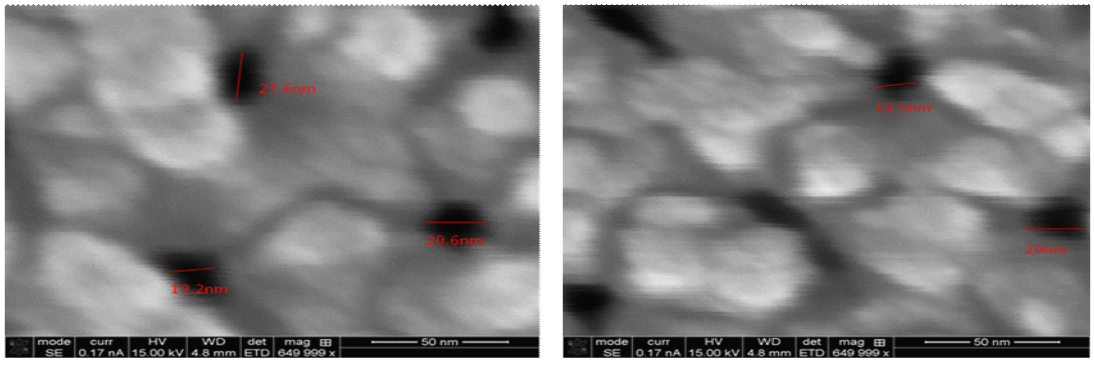

Figure 5.4 Proper magnification for measuring pore size of 35nm membrane and pore size measurement according to the scale

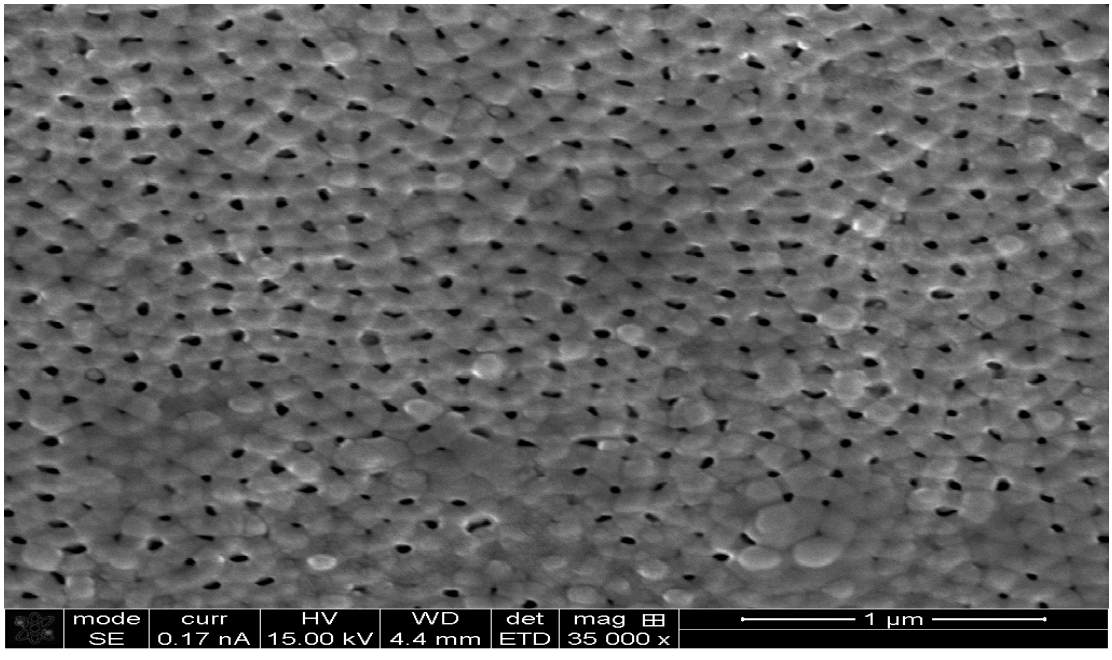

Figure 5.5 SEM of surface of 55nm membrane

For 55 nm membranes, we can get pore density of 19.5 pores/ 348644nm^2 and 116.5 pores/ 2178807nm^2 from Figure 5.6, thus the average pore density can be calculated as 5.49*10^{-5} pores/nm^2. In Figure 5.7 pore diameter is measured to have a average diameter of 52.6nm.

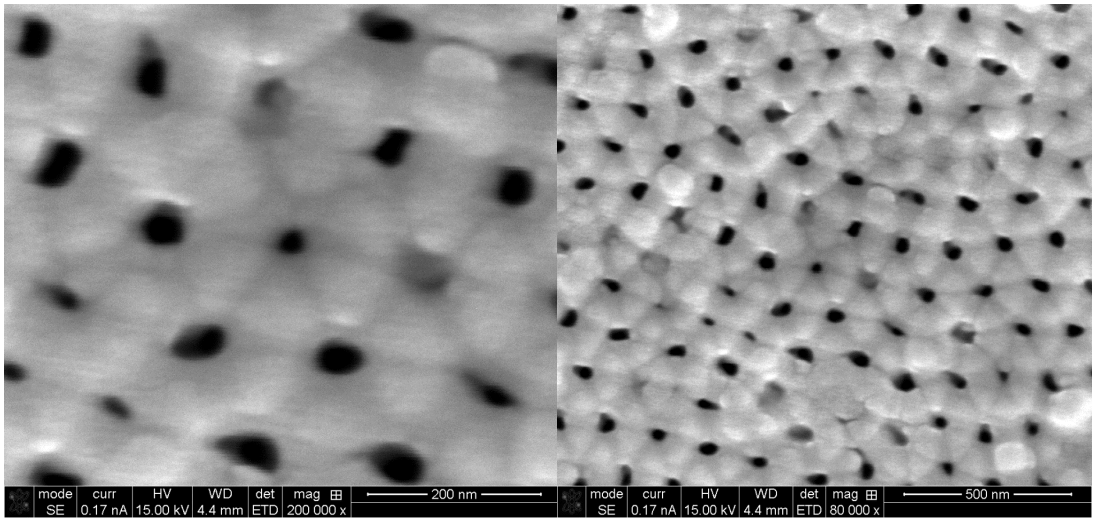

Figure 5.6 Proper magnification for pore density calculation of 55nm membrane

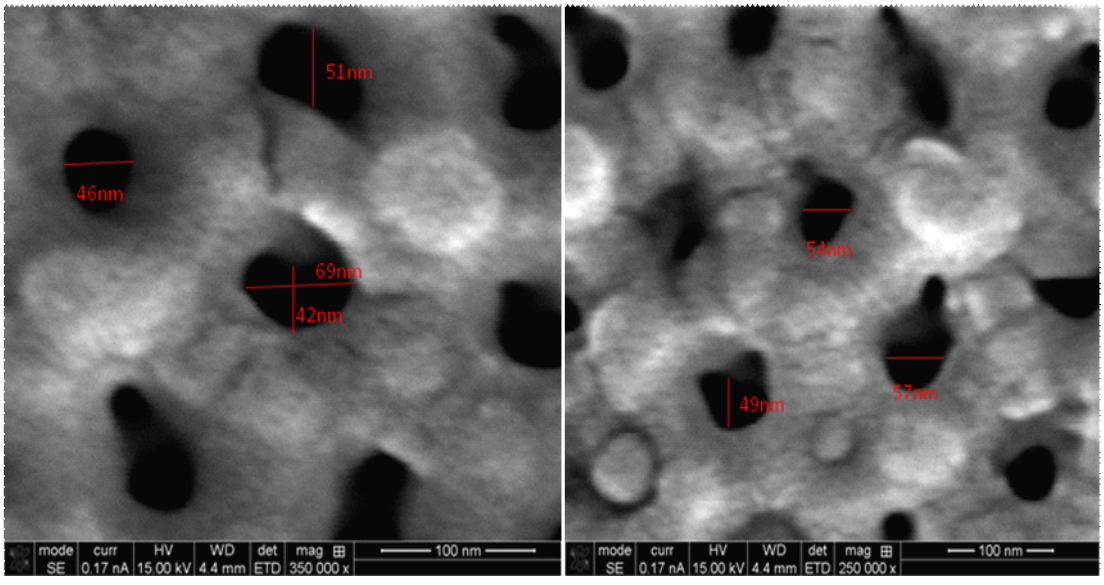

Figure 5.7 Proper magnification for measuring pore size of 55 nm membrane and pore size measurement according to the scale

As showed in Figure 5.8 100nm membrane has a even pore density and uniform pore size.

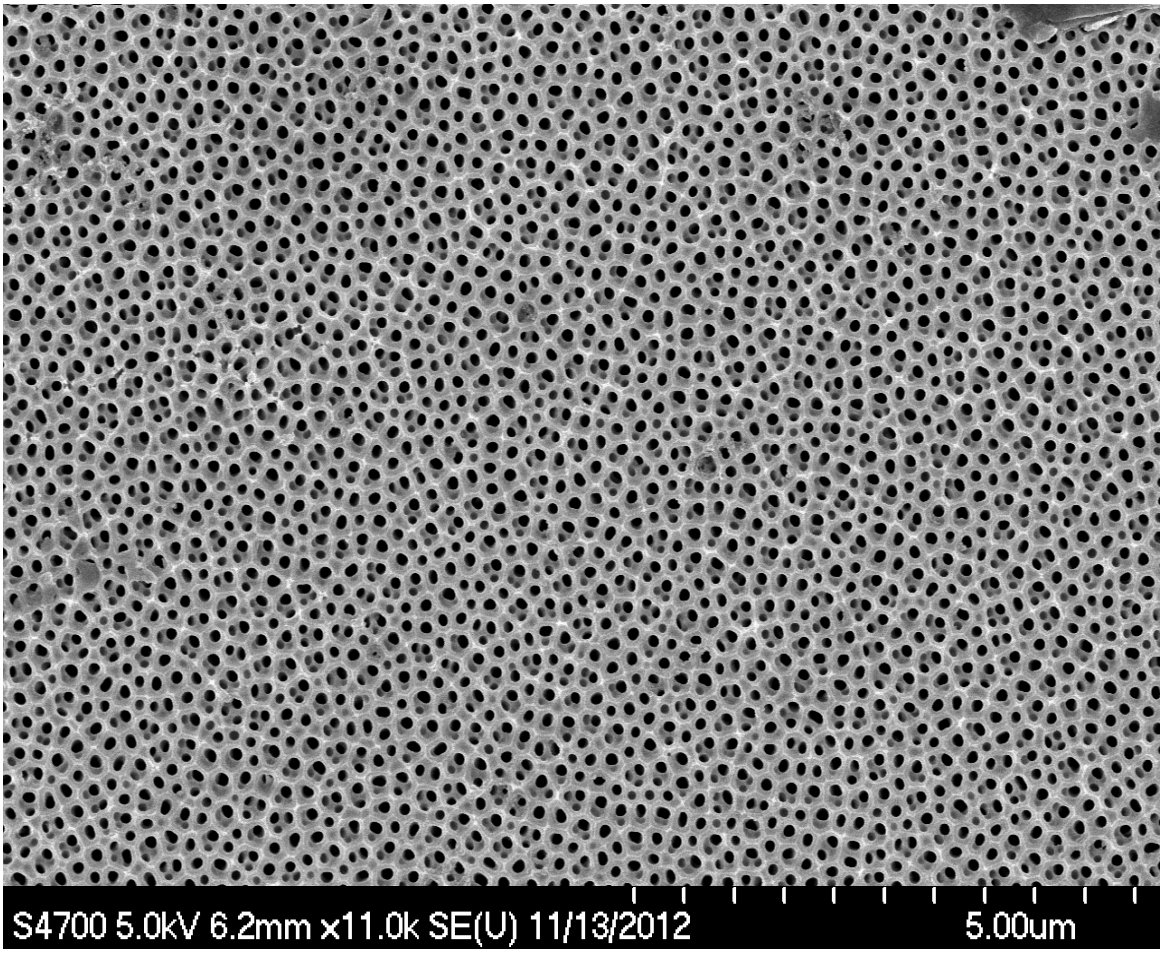

Figure 5.8 SEM of surface of 100nm membrane

For 100 nm membranes, pore densities are read as 30 pores/ 1114437nm2 and 55 pores/ 2131168nm2 from Figure 5.9, thus the average pore density can be calculated as 2.64e*10-5 pores/nm2. In Figure 5.10 pore diameter is measured and calculated to be 104.6nm. In Figure 5.10, the pore oblique can be easily tell on account of larger pore size and smaller magnification.

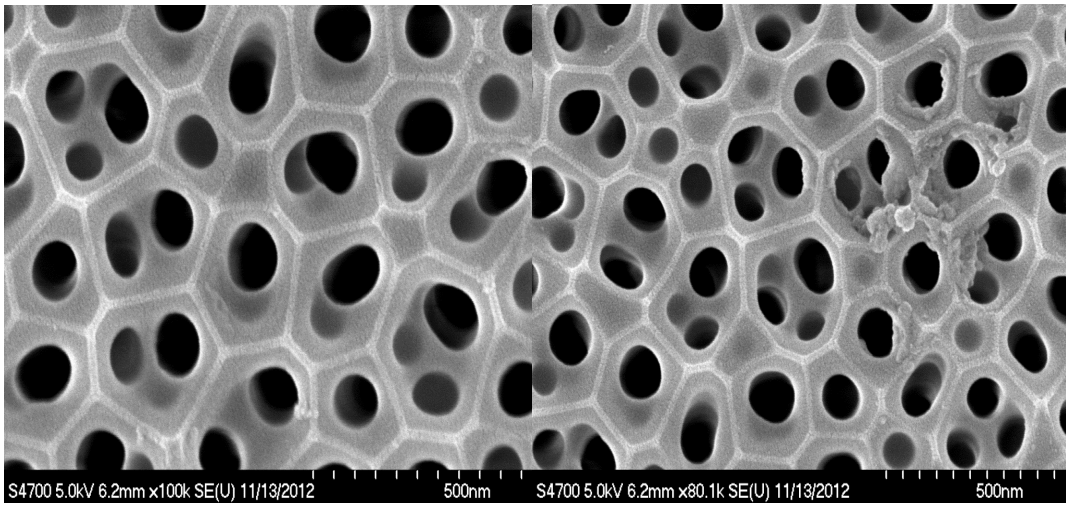

Figure 5.9 Proper magnification for pore density calculation of 100nm membrane

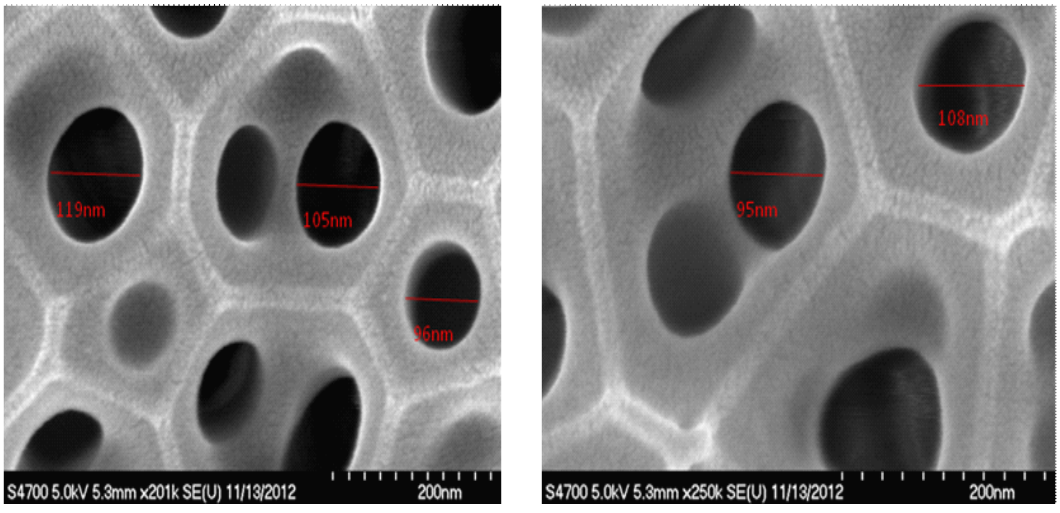

Figure 5.10 Proper magnification for measuring pore size of 100 nm membrane and pore size measurement according to the scale

5.2 KOZENY-CARMAN EQUATION APPROACH

Figure 5.1 indicates the pores are simply vertically penetrate through the membrane and Figure 5.2, 5.5 and 5.8 show that as sysmetric membranes, they can be considered as a bunch of nano-tube in parallel which simplify the porous model comparing to real core

samples. By using just characteristics from the core with no considerition of fluid properties, the simplified equation of Kozeny-Carman equation:

$$k = \frac{\phi\, d_p^2}{32\, \tau}$$

can be used in which Φ is the porosity of the porous media, d_p is the pore diameter and τ represents the tortuosity. In this case, Φ equals to the pore area divided by total area and τ=1. After calculation, results are showed in Table 5.1

Table 5.1 Permeability calculation using simplified Kezony-Carman equation

Membrane type	Pore density, Pores/nm^2	Pore diameter, nm	Permeability, md (based on simplified Kozeny-Carman equation)
35nm membrane	9.42*10^{-5}	19.8	0.00036
55nm membrane	5.49*10^{-5}	52.6	0.01
100nm membrane	2.64e*10^{-5}	104.6	0.078

5.3 PERMEABILITY TEST USING WATER

By using water pump to inject certain flow rate of de-ionized water into core-holder and measure pressure of both sides, permeability data are generated. Figure 5.11, 5.12 and 5.13 respectively show the pressure versus time after the changing of flow rate.

When the curve approaches horizontal which means the pressure doesn't change along with time, the steady-state is reached and the pressure data is taken to calculate the permeability.

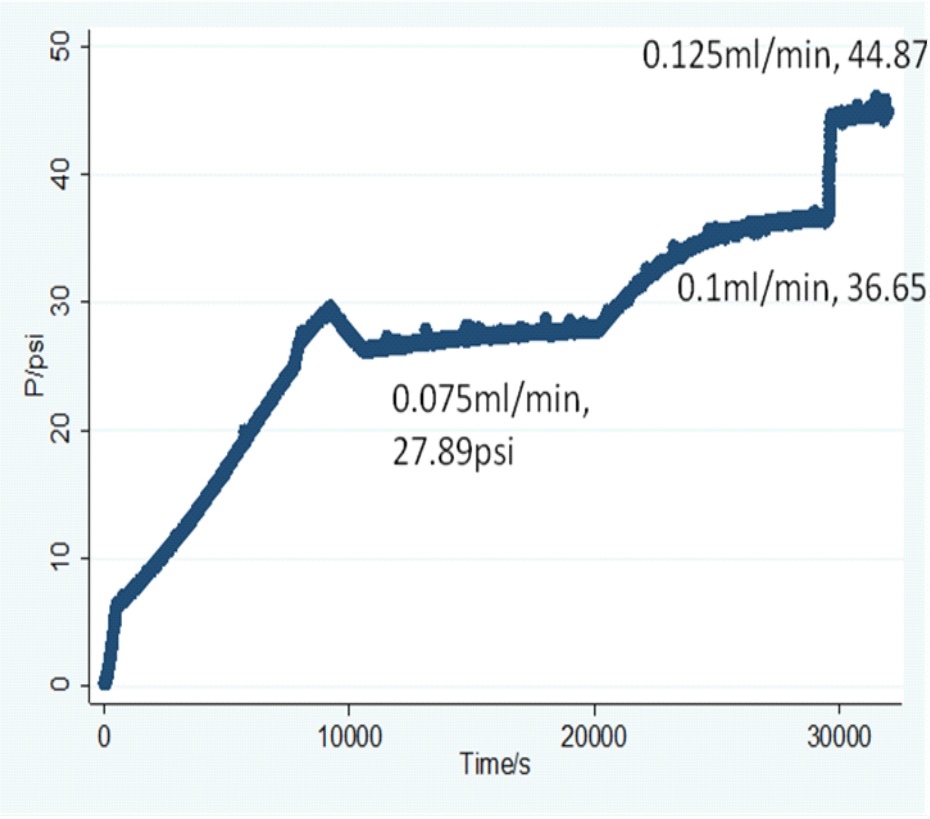

Figure 5.11 Water injection of 35nm(reading 20nm) membrane

30 to 60 minutes are reserved after the pressure data appear to be steady and over 300 data within 5 to 10 minutes are used to calculate the pressure in steady-state. The discontinuous data in Figure 5.13 are generated for the reason of accumulator refill because of the higher flow rate and the capability of accumulator.

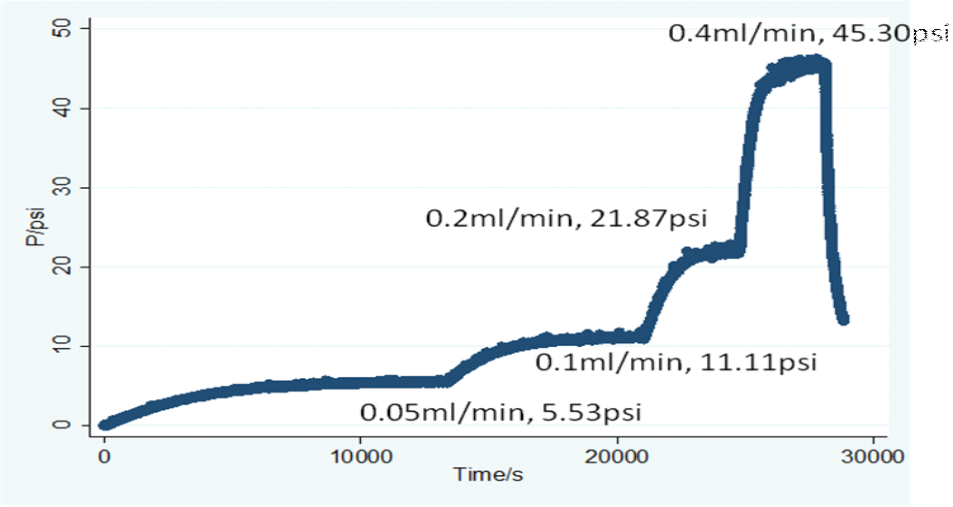

Figure 5.12 Water injection of 55nm(reading 52nm) membrane

After calculation using equation:

$$k = 1000 \frac{L}{A} \mu \quad Q \frac{1}{(P_o - P_i)}$$

Results of permeability measured by water injection method are showed in Table 5.2.

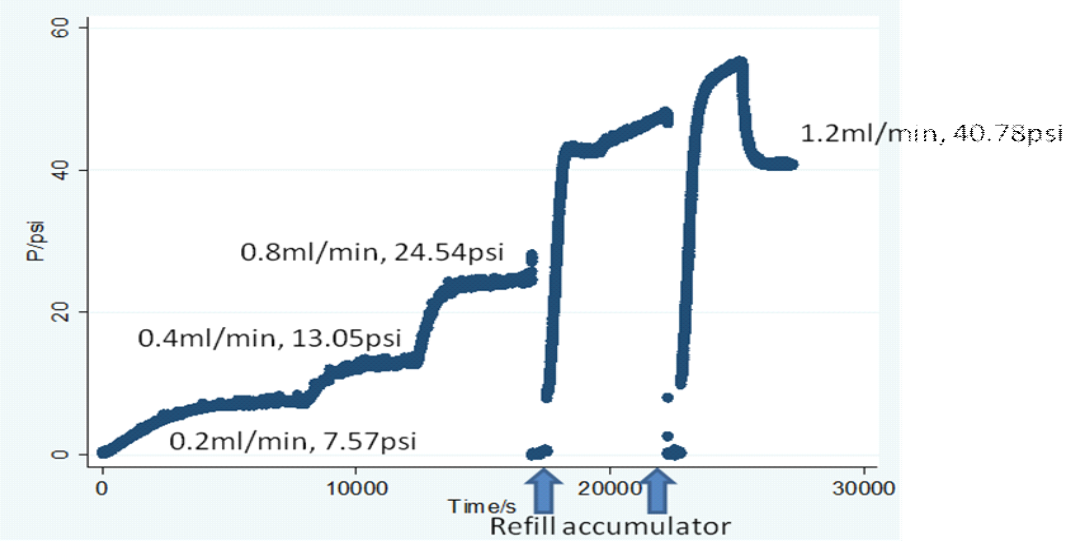

Figure 5.13 Water injection of 100nm(reading 104nm) membrane

The permeability results for 35(20)nm and 55(52)nm membranes are very uniform while those of 100(104)nm membrane are not that uniform but accaptable. After calcution, the average permeability results for three kinds of membranes are 0.0021, 0.0070 and 0.023md respectively.

Table 5.2 Collected and calculated lab data using water injection

Membrane type (reading pore size)	Flow rate, ml/s	Pressure, psi	Permeability, md	Average permeability, md
35nm (20nm)	0.075	27.89	0.0021	0.002135
	0.1	36.65	0.002131	
	0.125	44.87	0.002175	
55nm(52nm)	0.05	5.53	0.00706	0.007031
	0.1	11.11	0.007029	
	0.2	21.87	0.007141	
	0.4	45.3	0.006895	
100nm(104nm)	0.2	7.57	0.020631	0.02325
	0.4	13.05	.023935	
	0.8	24.54	0.025457	
	1.2	40.78	0.022979	

5.4 PERMEABILITY TEST CONSIDERING KLINKENBERG EFFECT

Core holder and Ultra Perm-600 is used to measure the flow rate of Nitrogen under different pressure drops. As for the membranes have nanoscale pore sizes, all sets of data

are analyzed by both Klinkenberg effect and Knudsen diffusion. Lab data collected by Ultra Perm-600 including pressures and flowrate are displayed in Table 5.3, 5.4 and 5.5.

Table 5.3 Core flooding test data using nitrogen of 35nm membrane

P1, atm	P2, atm	ΔP, atm	Q, ml/s	1/Pm, 1/atm	Ka, md
1.7488	0.9816	0.7672	0.671	0.732486	0.049277
2.0374	0.9864	1.0511	0.849	0.661414	0.04551
2.2886	0.9877	1.3009	0.996	0.61043	0.043136
2.4146	0.9864	1.4282	1.052	0.58807	0.041501
2.6093	0.9864	1.6229	1.155	0.556229	0.040098
2.8291	0.9857	1.8434	1.236	0.524268	0.037776
3.0647	0.9891	2.0756	1.312	0.493367	0.035614
3.2580	0.9884	2.2696	1.378	0.470984	0.034208
3.4200	0.9891	2.4309	1.428	0.453605	0.033097
3.9190	0.9898	2.9292	1.585	0.407433	0.030486
3.9067	0.9905	2.9163	1.579	0.408396	0.030505
3.4656	0.9898	2.4758	1.439	0.448892	0.032746
2.8060	0.9857	1.8203	1.217	0.527469	0.037668
2.3336	0.9850	1.3485	1	0.602667	0.041779

Note: P1 is upstream pressure, P2 is downstream pressure, ΔP is pressure difference, Q is flowrate of nitrogen, 1/Pm is the reciprocal of average pressure and Ka is apparent permeability

1/Pm and Ka are calculated for gas slippage curve which also known as Klinkenberg effect curve in following equation:

$$\frac{1}{P_m} = \frac{2}{P_1 + P_2}$$

$$K_a = \frac{2000 \times L \times \mu \times P_m \times Q}{S \times (P_1^2 - P_2^2)}$$

Table 5.4 Core flooding test data using nitrogen of 55nm membrane

P1, atm	P2, atm	ΔP, atm	Q, ml/s	1/Pm, 1/atm	Ka, md
2.0579	0.8993	1.1586	1.201	0.676335	0.058402
2.5589	0.9027	1.6562	1.495	0.577778	0.050856
3.0170	0.9061	2.1110	1.745	0.509804	0.046573
3.5017	0.9081	2.5936	1.984	0.453535	0.043098
4.2791	0.9190	3.3601	2.276	0.384756	0.038163
5.1082	0.9258	4.1824	2.564	0.331453	0.034539
4.7332	0.9210	3.8121	2.424	0.35372	0.035825
3.9333	0.9142	3.0191	2.136	0.412583	0.039861
2.9748	0.9081	2.0667	1.709	0.515077	0.046589

In consideration of the sensitive of the membranes due to the small pore size, during the measurement of flowrate change with the change of pressure difference, upstream

pressure is switch up first to build a series of pressure difference and then switch down to see wether the operation cause the change on the membrane by either plugging the pores to reduce permeability or fracturing the membrane leading to a larger permeability. The data show a great repeatability to give the evidence that the membranes didn't receive any effect to cause error by the operation.

Table 5.5 Core flooding test data using nitrogen of 100nm membrane

P1, atm	P2, atm	ΔP, atm	Q, ml/s	1/Pm, 1/atm	Ka, md
4.5793	1.0027	3.5766	5.097	0.080292	3.486899
5.3356	1.0531	4.2825	6.137	0.080739	3.990798
6.3329	1.1436	5.1892	7.319	0.079464	4.670318
7.1654	1.2362	5.9292	8.202	0.077938	5.248208
8.2505	1.3792	6.8713	9.165	0.075147	6.015325
9.1443	1.5187	7.6256	9.67	0.071446	6.660827
10.2777	1.7216	8.5562	10.294	0.067784	7.495556
11.3519	1.9401	9.4118	10.892	0.065201	8.303071
12.7733	2.2614	10.5119	11.636	0.062366	9.391664
10.4438	1.7529	8.6909	10.387	0.067336	7.618873
8.7577	1.4520	7.3057	9.416	0.072616	6.377623
7.1484	1.2280	5.9204	8.165	0.077702	5.232474
5.5916	1.0688	4.5228	6.491	0.080859	4.160465

With the precondition of considering the gas diffusion as Darcy's flow and following Klinkenberg correction, gas sllipage curve can be generated with reciprocal of average pressure and apparent permeability in Figure 5.14, 5.15 and 5.16. The intersection of the curve and Y axis represents the absolute permeability.

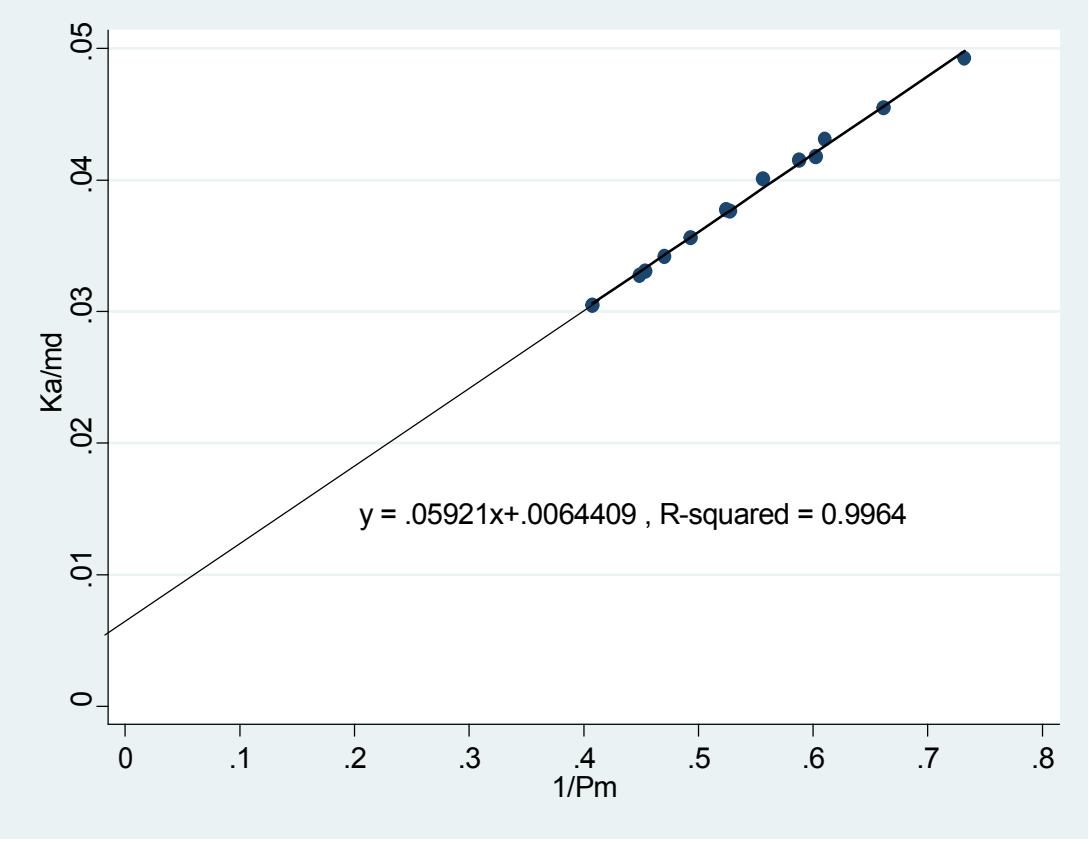

Figure 5.14 Slippage curve of nitrogen flow through membrane with pore size of 20nm

Figure 5.14 shows a great correlation between permeability and reciprocal of average pressure. The good linear regression has an interception with Y axis of 0.064 which indicates the absolute permeability using gas method considering Klinkenberg effect for 20nm membrane.

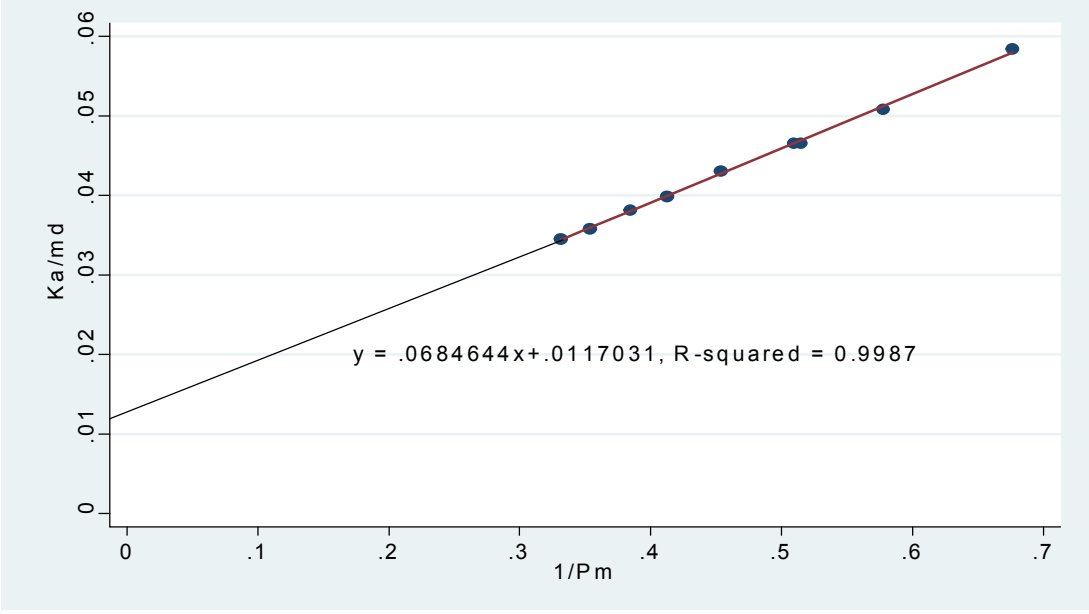

Figure 5.15 Slippage curve of nitrogen flow through membrane with pore size of 52nm

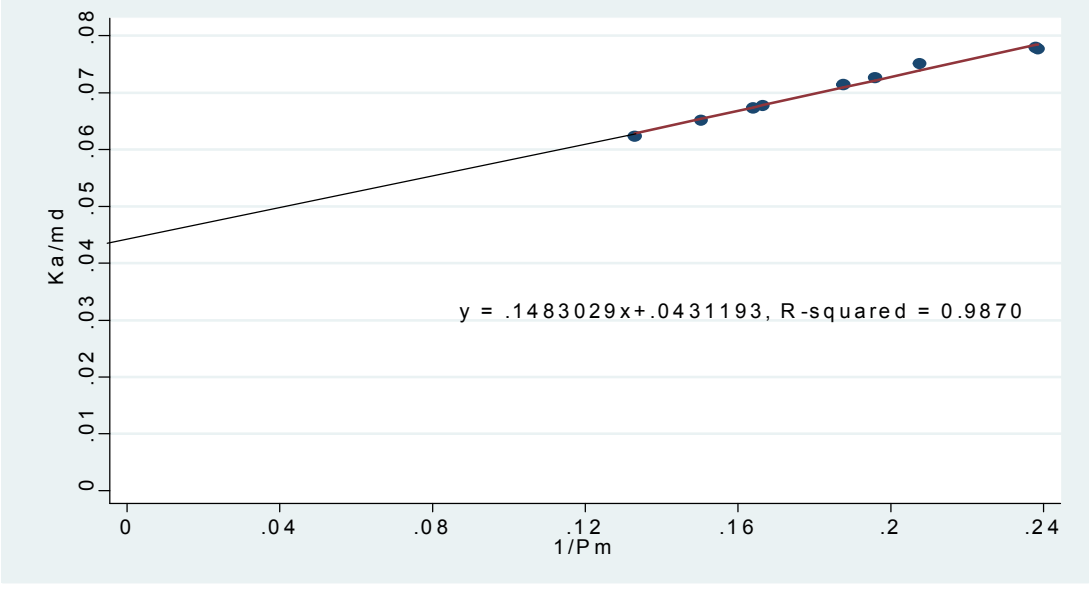

Figure 5.16 Slippage curve of nitrogen flow through membrane with pore size of 104nm

All three figures above show a great linear regression of the data. The coefficient of determination reaches as high as 0.9987 in Figure 5.8 and the smallest coefficient of determination is 0.987 which is also good enough for a linear regression. From the

readings of intersections of the three figure, 0.0064md, 0.0117md and 0.0432md are the abosulte permeability of 20nm, 52nm and 104nm membrane respectively with the precondition of considering the gas diffusion as Darcy's flow and following Klinkenberg correction.

5.5 COMPARISON BETWEEN THREE CALCULATION METHODS

After getting all the permeability data using three different methods: Kezony-Carman equation, Water injection and Nitrogen core flooding test considering slippage flow, a comparison between three methods on membranes with different pore size is showed in Figure 5.17

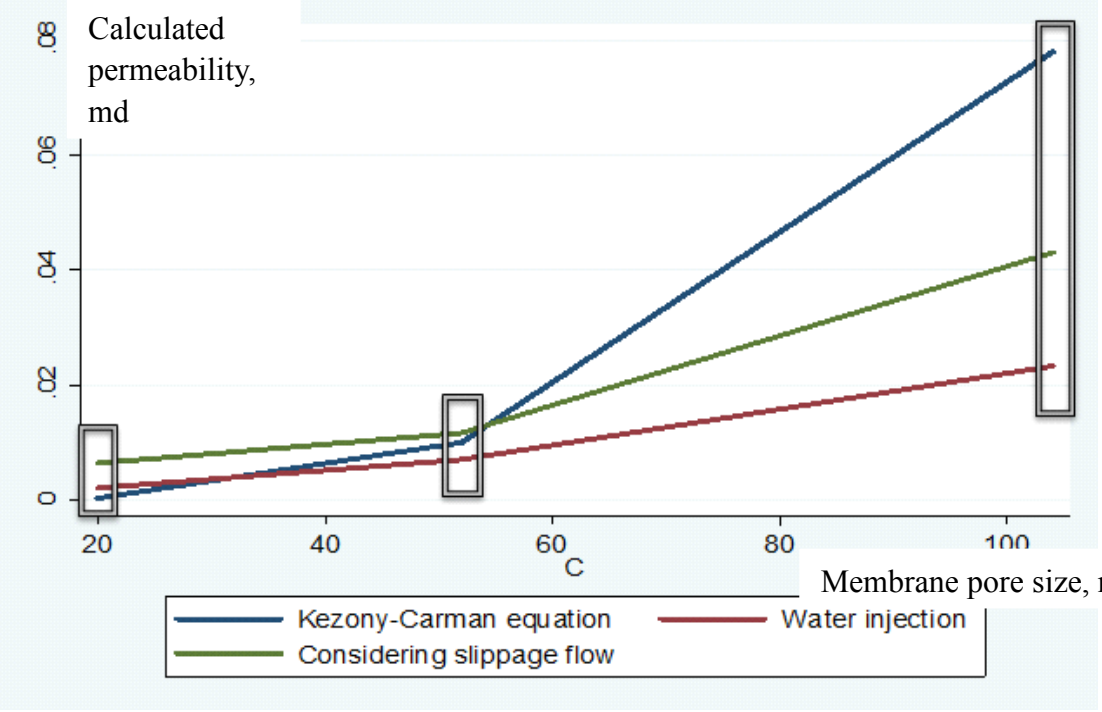

Figure 5.17 Comparison between three permeability calculation method

Water injection and gas measurement using Darcy's law and slippage effect have similar trend besides permeability get from water injection is slightly less than permeability data from nitrogen measurement. Permeability values from all three differenct methods are quite closer in membranes with smaller pore sizes but more separated when it gets to 104nm. All three of them are in same magnitude.

5.6 LAB DATA FITTING INTO EXISTING NANOFLOW MODELS

5.6.1 Florence Micoflow Model. The new microflow model represents gas flow in low permeability core samples and is also applied as a correlation for prediction of the equivalent liquid permeability in much the same fashion as the Klinkenberg model. Table 5.6 is accomplished after fitting lab data into Florence microflow model for gas flow in idealed medium by following equation:

$$k_a = k_\infty \left[1+\alpha(Kn)Kn\right]\left[1+\frac{4Kn}{1+Kn}\right]$$

From Table 5.6, calculated permeability values using Florence equation range from negative tens of thousands to positive tens of thousands. Clearly lab data doesn't fit the Florence microflow model. Though Kn values used in deriving of Florence model are from 0.1 to 1 which are much smaller than Kn values of the nanoscale membranes which range from $5*10^4$ to $1*10^6$.

The magnitude of the Knudsen number determines the appropriate gas dynamic regime. When the Knudsen number is small compared to unity, of the order of Kn ≤ 0.1,

the fluid can be treated as a continuous medium and described in terms of the macroscopic variables: velocity, density, pressure and temperature. In the transition flow regime, for Knudsen numbers of the order of unity or greater, a microscopic approach is required, wherein the trajectories of individual representative molecules are considered, and macroscopic variables are obtained from the statistical properties of their motions. In both internal and external flows, for Kn $\geq$ 10, intermolecular collisions in the region of interest are much less frequent than molecular interactions with solid boundaries, and can be ignored. Flows under such conditions are termed collisionless or free molecular. In the range 0.1 $\leq$ Kn $\leq$ 1.0, termed the slip flow regime, it is sometimes possible to obtain useful results by treating the gas as a continuum, but allowing for discontinuities in velocity and temperature at solid boundaries.

Table 5.6 Permeability calculation by Florence microflow model

35-2	55-2	100-2
-3970.3	-52349	-566.57
347764	3659.49	1493.93
-80968	4400.39	18845.8
-50686	1267.01	705.983
-2586.6	1893.03	-1808.6
-50820	3942.92	365.71
6856.88	-11916	436.59

5.6.2 Javadpour Model. The permeability in Javadpour model is not only a property of the rock system, but it also depends on properties of flowing gas at specified pressure and temperature. This dependence was expected from the beginning because interaction of different gases with the solid matrix is one of the parameters that was included in the model. Also, the model integrates Knudsen diffusion, which is negligible for conventional systems, plays an important role in unconventional reservoirs.

After fitting lab data into Javadpour's model, a comparison between lab data considering Klinkenberg effect and theoretical value gathered from Javadpour's equation was conducted. The differences between lab data and calculated values by Javadpour model are showed in following figures.

Figure 5.18 shows a significant difference between lab data of 20nm membrane and Javadpour model. Lab data are several times larger than Javadpour model.

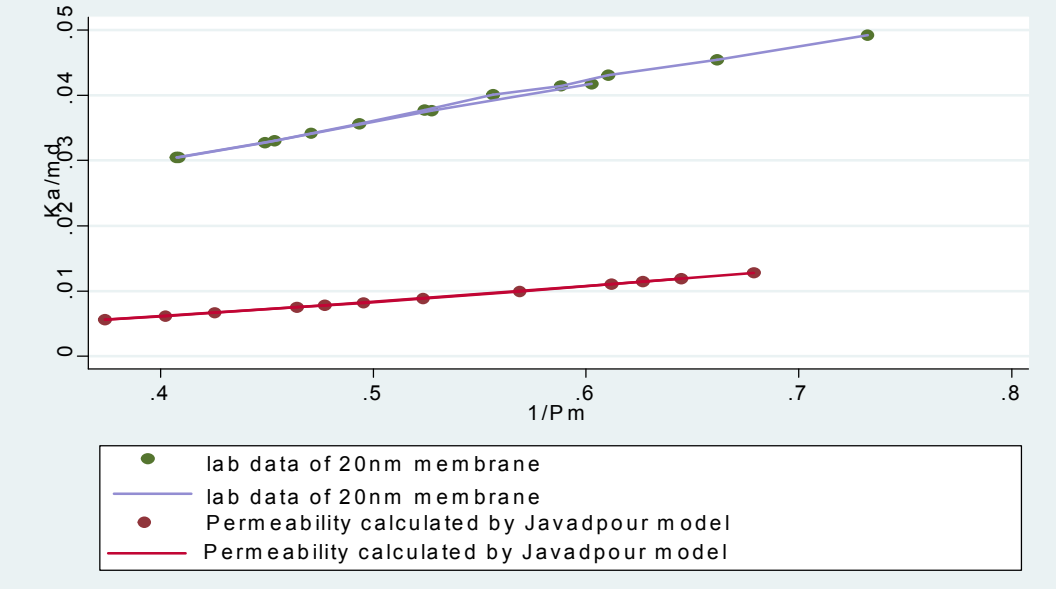

Figure 5.18 Comparison between lab data of 20nm membrane and Javadpour model

Data are pretty close to each other in Figure 5.19 and 5.20 with a slight difference of trend. The lab data have smaller trend than that of Javadpour model and the two linear lines have a interception at some point.

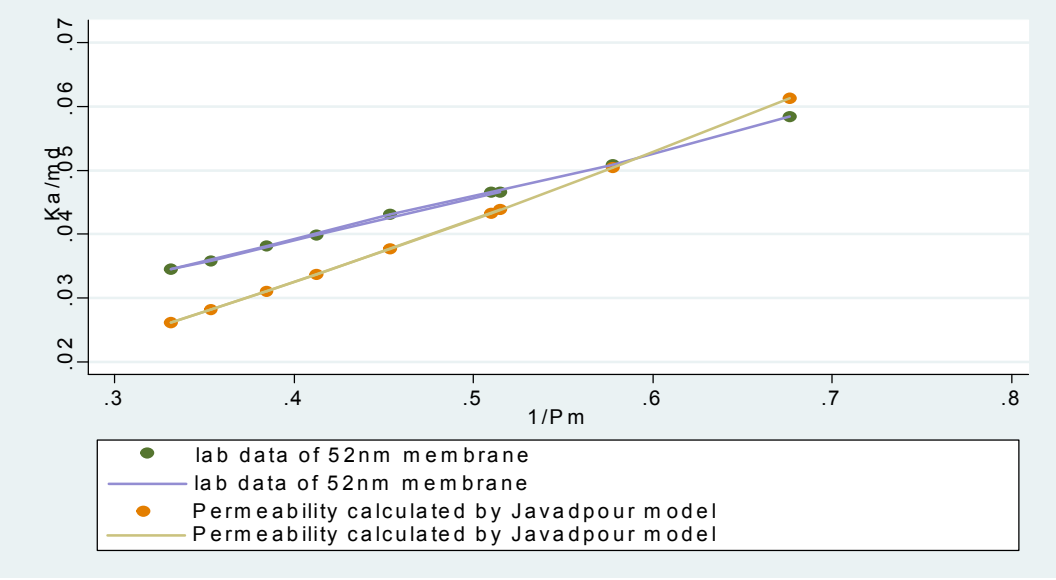

Figure 5.19 Comparison between lab data of 52nm membrane and Javadpour model

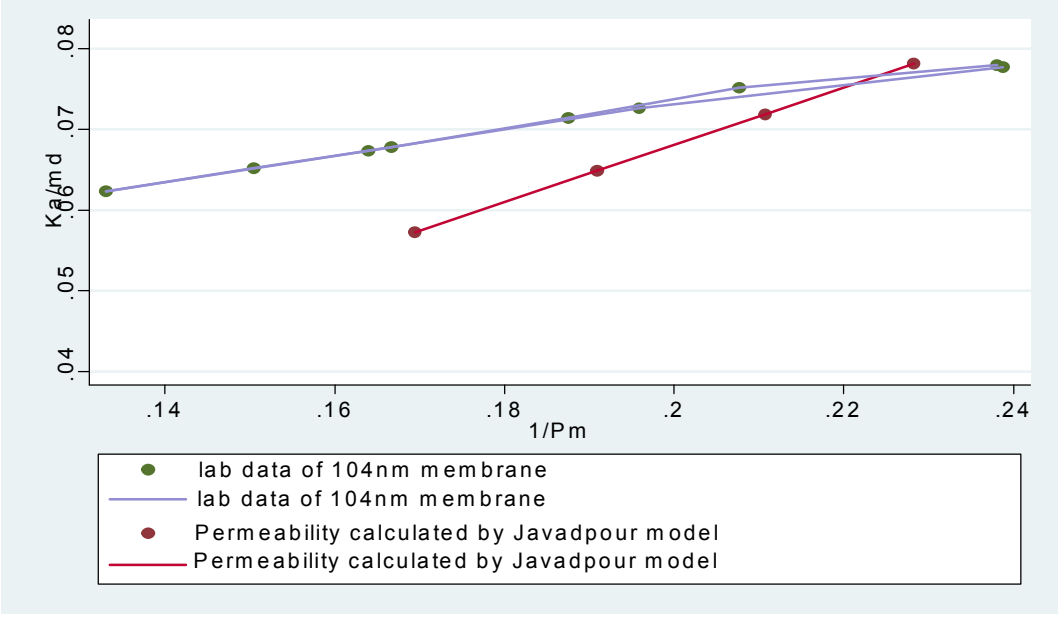

Figure 5.20 Comparison between lab data of 104nm membrane and Javadpour model

To compare the Javadpour model and absolute permeability gathered by water injection and also by Kozeny-Carman equation, Javadpour model curves are extended to seek the intersection with Y axis in conditions of three different pore sizes. However the intersection between Javadpour model curve and Y axis are -0.0039, -0.0079 and -0.004 respectively.

6. CONCLUSION AND FUTURE WORKS

6.1 CONCLUSIONS

1. All the ceramic membranes have relatively uniform pore density and pore size.

2. Permeability calculation based on physical characterization of the media gives the result of 3.6e-4md for 20nm membranes, 0.01md for 53nm membranes and 0.078nm for 105nm membranes.

3. Permeability measured from water flooding test shows the results of 0.002md, 0.007md and 0.023md for 20nm, 53nm and 105nm membranes respectively.

4. Even though with the tiny pore size equivalent to shale, all the membranes seem to be able to fit a Klinkenberg correction which lead to values of 0.006md, 0.011md and 0.043md.

5. Permeability get from gas measurement calculated by Klinkenberg correction, water measurement and calculation based on pore distribution are slightly different within ths same magnification.

6. Knudsen number can reach as much as the magnitude of million with pore size of nanometer which means Knudsen diffusion should appear instead of Klinkenberg diffusion under such condition.

7. Florence equation not suitable for this lab data due to the oversized Knudsen number.

8. Javadpour's equation can better fit the Ka calculated by Darcy's law from lab data using appropriate tangential momentum accommodation coefficient.

6.2 RECOMMENDED FUTURE WORK

1. The results indicate that even in 20nm scale Klinkenberg effect still seems to be existed. More work to distinguish Slippage diffusion and Knudsen diffusion need to be done by a). using smaller scale pore size or b). using gas with larger molecule diameter.

2. Futher detailed research could be focused on the transition zone between Slippage and Knudsen diffusion. Assuming two kinds of diffusion gradually and successively appear and disappear under certain Knudsen number, the transition zone could be qualified precisely. The controlling of the factors tempereture and pressure, or even using gas with different molecule diameter might achieve such goal.

3. Model to describe fluid flow in nanoscale porous media instead of single nano tube should be set up by lab data and fluid flow equations. The correlation between practical index pressure and flowrate need to be established to apply to industrial production.

REFERENCES

A Sakhaee-pour, S Bryant, Gas permeability of shale, SPE 146944, (2011)

AJ Mallon, RE Swarbrick, How should permeability be measured in fine-grained lithologies? Evidence from the chalk, Geofluids, (2008)

BE Law, JB Curtis Introduction to unconventional petroleum systems, AAPG bulletin, (2002)

Bird, G. A. Molecular gas dynamics and the direct simulation of gas flows, Clarendon Press: New York, (1994)

Bird, R.B., Stewart, W.E. and Lightfood, E.N., Transport Phenomena; Second Edition, John Wiley & Sons, (2007)

Brown, G.P., Dinardo, A., Cheng, G.K. and Sherwood, T.K., The Flow of Gases in Pipes at Low Pressures; Journal of Applied Physics, (1946)

C Cipolla, E Lolon, J Erdle, B Rubin, Reservoir modeling in shale-gas reservoirs, SPE 125530, (2010)

CK Ho, SW Webb, Gas transport in porous media, (2006)

Cooper, S.M., Cruden, B.A., Meyyappan, M., Raju, R. and Roy, S., Gas Transport Characteristics through a Carbon Nanotubule; Nano Letters, (2003) Department of Energy, U.S. Shale Gas and Shale Oil Plays, (2011)

DL Luffel, CW Hopkins, Matrix permeability measurement of gas productive shales, SPE 26633, (1993)

D Silin, T Kneafsey, Gas Shale: From Nanometer-scale Observations to Well Modeling, Canadian Unconventional Resources, (2011)

F Florence, J Rushing, K Newsham, Improved permeability prediction relations for low permeability sands, SPE 107954, (2007)

F Civan,CS Rai, CH Sondergeld, Shale-gas permeability and diffusivity inferred by improved formulation of relevant retention and transport mechanisms, Transport in Porous Media, (2011)

F. Javadpour, Nanopores and Apparent Permeability of Gas Flow in Mudrocks (Shales and Siltstone) Journal of Canadian Petroleum Technology, (2009)

F. Javadpour, D. Fisher and M. Unsworth, Nanoscale Gas Flow in Shale Sediments, Journal of Canadian Petroleum Technology, (2007)

FOLK, R.L., Petrology of Sedimentary Rocks; Hemphill Publishing Company, (1974)

F Wang, R Reed, Pore networks and fluid flow in gas shales, SPE 1234253, (2009)

GE Karniadakis, A Bes kk, NR Aluru, Microflows and nanoflows: fundamentals and simulation, (2005)

Hadjiconstantinou, N.G., The Limits of Navier-Stokes Theory and Kinetic Extensions for Describing Small Scale Gaseous Hydrodynamics; Physics of Fluids, (2006)

Heid, J.G., et al., Study of the Permeability of Rocks to Homogeneous Fluids, in API Drilling and Production Hornyak, G.L., Tibbals, H.F., Dutta, J. and Moore, J.J., Introduction to Nanoscience and Nanotechnology; CRC Press, (2008)

JEANS, J.H., The Dynamical Theory of Gases; Dover Publications, Inc., New York, NY, (1954)

Joël Billiotte, Diansen Yang, Kun Su, Experimental study on gas permeability of mudstones, Physics and Chemistry of the Earth, (2008)

Jones, F.O. and Owens, W.W., A laboratory Study of Low Permeability Gas Sands, paper SPE 7551, (1979)

Jones, S.C., Using the Inertial Coefficient to Characterize Heterogeneity in Reservoir Rock, paper SPE 16949, (1987)

Karniadakis, G., Beskok, A. and Aluru, N., Micro-flows and Nanoflows: Fundamentals and Simulation, Springer Science Business Media, (2005)

Katsube, T.J., Shale Permeability and Pore Structure Evolution Characteristics, Geological Survey of Canada, (2000)

Klinkenberg, L.J., The Permeability of Porous Media to Liquid and Gases, paper presented at the API 11th Mid Year Meeting, Tulsa, Oklahoma (May 1941); in API Drilling and Production Practice (1941)

Kundt, A. and Warburg, E., Über Reibung und Wärmelei-tung verdünnter Gase, Poggendorfs Annalen der Physik und Chemie, (1875)

MK Hubbert, Darcy's law and the field equations of the flow of underground fluids, Hydrological Sciences Journal, (1957)

Malek Elgmati; Hao Zhang; Baojun Bai, Ralph Flori, Submicron-Pore Characterization of Shale Gas Plays, SPE 144050, (2011)

Magonov, S. and Whangbo, M.-H., Surface Analysis with STM and AFM: Experimental and Theoretical Aspects of Image Analysis; VCH Publishers, (1996)

Maxwell, J.C., The Scientific Letters and Papers of James Clerk Maxwell, (1995)

Philip H. Nelson, Pore-throat sizes in sandstones, tight sandstones, and shales, GEOLOGIC NOTE, (2009)

Q Chen, W Kinzelbach, C Ye, Y Yue, Variations of permeability and pore size distribution of porous media with pressure, Journal of Environmental Quality, (2002)

R Ambrose, R Hartman, New pore-scale considerations for shale gas in place calculations, SPE 131772, (2010)

R.G. Loucks, R.M Reed., S.C. Ruppel and D.M. Jarvie, Morphology, Genesis, and Distribution of Nanometer-Scale Pores in Siliceous Mudstone of the Mississippian Barnet Shale, Journal of Sedimentary Rocks, (2009)

R Bustin, A Bustin, A Cui, D Ross, Impact of shale properties on pore structure and storage characteristics, SPE119892, (2008)

RM Flores, Coalbed methane: from hazard to resource, International Journal of Coal Geology, (1998)

Roy, S., Raju R., Chuang, H. F., Cruden B. A., Meyyappan M. J., Modeling gas flow through microchannels and nanopores, Appl. Phys. (2003)

Sampath, K. and Keighin, C.W., Factors Affecting Gas Slippage in Tight Sandstones, paper SPE 9872, (1981)

SA Reinecke, BE Sleep, Knudsen diffusion, gas permeability, and water content in an unconsolidated porous medium, Water Resources Research, (2002)

S Motealleh, SL Bryant, Predictive model for permeability reduction by small wetting phase saturations, Water Resources Research, (2007)

Stuart A Cox, David M Cook, Ken Dunek, Reagan Daniels, Unconventional Resource Play Evaluation: A Look at the Bakken Shale Play of North Dakota, SPE 114171 (2008)

V Bust, A Majid, J Oletu, P Worthington, The Petrophysics of Shale Gas Reservoirs: Technical Challenges and Pragmatic Solutions, IPTC 14631, (2011)

W.J. Haskett, SPE, and P.J. Brown, Evaluation of Unconventional Resource Plays, SPE 96879 (2005)

X Cui, AMM Bustin, RM Bustin, Measurements of gas permeability and diffusivity of tight reservoir rocks: different approaches and their applications, Geofluids, (2009)

VITA

Songyuan Liu was born in Heilongjiang, China. He received his Bachelor of Science degree in Biology from Fudan University in 2011. He started self-learning Petroleum Engineering and worked as a research assistant in China University of Petroleum and Northeast Petroleum University in China from the year 2010. He received his Master's degree in Petroleum Engineering from Missouri University of Science and Technology at Rolla, Missouri in May 2013.